NTNU
Innovation and Creativity

Vehicle velocity estimation on non-flat roads

Stian Nerbråten

Master of Science in Engineering Cybernetics
Submission date: May 2007
Supervisor: Tor Arne Johansen, ITK

Norwegian University of Science and Technology
Department of Engineering Cybernetics

Problem Description

The trend is that modern cars are being equipped with increasingly advanced active safety systems. These typically need accurate information about vehicle velocity, which is hard and expensive to measure directly. On SINTEF/NTNU a computationally efficient nonlinear observer for vehicle velocity estimation has been developed, but its performance on non-flat roads leaves something to be desired. Thus, the task of the student is to extend the observer to cope with non-flat roads, by also using other measurements. In view of the increasing availability of navigation systems in cars most emphasis is put on GPS measurements, but also other measurements such as inclination sensors, pressure sensors in active suspension systems (ABC), etc. are interesting.

1. Perform brief litterature review of bank- and/or inclination angle estimation in automotive settings. Important issues are purpose of estimation (e.g. velocity estimation for ESC), accuracy, if available, and types of sensors used.
2. Describe the sensors that are chosen, and how they give information about vehicle velocity or road bank and inclination angles.
3. Develop velocity observer concepts for non-flat roads
   a. Design and analyze the concepts
   b. If possible, analyze robustness of the design
   c. Implement and test the observer on real measurement data

Assignment given: 08. January 2007
Supervisor: Tor Arne Johansen, ITK

Preface

This report is a Master's Thesis written at the Departement of Engineering Cybernetics (ITK), Norwegian University of Science and Technology (NTNU). The work is part of the ongoing European Commission STREP project Complex Embedded Automotive Control Systems (CEmACS), in which SINTEF ICT and DaimlerChrysler participate.

CEmACS concerns active safety systems for cars. Since one of the main criteria for achieving reliable control is having good state estimates, the development of a nonlinear observer for vehicle velocity is part of the project. This report deals with the idea that standard GPS and roll rate measurements can be integrated with the observer to yield higher accuracy when the vehicle is subjected to disturbing elements like road grade and bank angle.

I would like to thank Dr. Lars Imsland (SINTEF ICT), Professor Tor Arne Johansen and Phd. student Håvard Fjær Grip for invaluable guidance and discussions during this final year as a student. Special thanks go to Dr. Jens C. Kalkkuhl and Mr. Avshalom Suissa (DaimlerChrysler Research and Technology, Stuttgart) for providing resources necessary for testing and validation.

Trondheim, May 31, 2007

Stian Nerbråten

Contents

Summary

The main purpose of this report, is to evaluate feasibility of using The Global Positioning System as an aiding tool for vehicle state estimation based on nonlinear techniques, and to develop a potential solution to the road bank angle problem. Previous work within the CEmACS project, includes development of a general nonlinear observer for lateral and longitudinal velocity, and an augmentation in the form of road-tire friction adaptation. Because the existing solutions have been shown to lack robustness with regards to certain disturbances, such as road grade and road bank angle, it has been stated that the estimation scheme should be upgraded, so that these disturbances can be accounted for. By including GPS velocity or a or a roll rate gyro measurement in the observer feedback loop, the possibility of detecting previously inobservable quantities is gained. In simple terms, evaluation of feasibility corresponds to demonstrating improvements and limitations of new solutions, using relatively crude methods in the test procedures.

Problems related to the above mentioned task, are approached by means of signal processing and control theory. Following an intuitive sequence of operations, the report presents GPS theory and results first, as this lays the foundation for all subsequent results. Methods used comprise simple differentiaton, rotational kinematics and discrete filtering. Secondly, theory and results related to nonlinear observers, with focus on GPS aiding, are examined thoroughly. Lyapunov theory, known from control engineering, is used to evaluate stability, while data from simulations and actual vehicle tests is used to show how a new observer scheme can improve existing solutions.

Before the most important results are presented, something should be said about their accuracy and significance. It has already been pointed out that the methods used are not based on optimality requirements, and consequently the results are best viewed as indicators of potential, rather than absolute solutions. This is especially true for the GPS velocity calculations, which are based on differentiation of position measurements; generally not a desired approach.

In this report, it is firstly shown that GPS position measurements can be used to compute receiver velocity in the body-fixed coordinate frame. While this is a crude approach, resulting in relatively poor signal to noise ratio, it is easily implemented on low-level equipment. It is also shown that it is possible to use these velocities as measurements in a nonlinear observer structure, slightly modified from previous solutions within the CEmACS project. By doing this, accurate estimates of road grade and bank

angle are achieved, so long as these vary slowly enough. Stability of the observer is not proven in the general sense, but it is shown that it can be made stable through realistic assumptions and gain selection. Stability is further demonstrated through the use of data sets from actual vehicle tests.

Secondly, a mathematical model of roll dynamics is combined with a roll rate measurement to create the possibility of detecting road bank angle. This is done by the now familiar nonlinear observer approach. Usefulness is demonstrated by simulations, but no stability proof is presented.

The main conclusion is that it is feasible to use GPS aiding to account for robustness problems in a vehicle state estimation scheme, and that the inclusion of a roll rate measurement opens up possibilities for "cheap" bank angle detection. A direct implementation of results presented in the report may not be ideal, but the fact that the system works for a large set of conditions, suggests that it is worthwhile to develop it further. This is especially true when it is assumed that GPS receivers will become an integral part of new vehicles in the near future. Refinements and upgrades can be made in the form of more advanced GPS technology, new parameter estimation techniques and integration with the road-tire friction adaptation scheme.

Chapter 1

Introduction

Over the last decade, two separate technologies have played lead roles in changing our perception of what a car and its computer system is capabale of doing. Active safety systems help the driver cope with potentially dangerous situations, or to avoid them altogether. Fitting the car with a Global Positioning System (GPS) receiver and digital maps, makes it possible for the driver to navigate accurately based on computer generated instructions. The first of these has a direct influence on how dangerous an unwanted driving situation becomes, while the other is more of a perk, potentially increasing safety by allowing the driver to concentrate on operating the vehicle. Lately, however, it has been suggested that a powerful tool such as GPS should be integrated with the safety system in order to achieve greater accuracy of estimates, and even give information about previously inobservable states or disturbances.

A GPS system is typically much more expensive than standard measurement devices used for vehicle state estimation. As the financial aspects of serial production apply tight constraints with regards to cost of equipment, an estimation scheme reliant on GPS measurements is not desired. However, cars that ship with GPS receivers should be able to take advantage of the new or redundant information such a system provides.

As the name clearly states, GPS is a position determination system, specifically designed for dynamic navigation purposes. The convenient irony here, is that with regards to accuracy, speed determination is what GPS does best. Active safety systems, e.g. ESP [1], which is a yaw stabilization system, uses vehicle velocity information in the feedback loop. Direct measurement of velocity is typically done with costly instruments, and is consequently not a viable solution. The standard approach to velocity estimation has been (extended) Kalman filtering, as in [2], using acceleration and yaw rate measurements as input. The drawback with this approach is that the Kalman filter (KF) is computationally inefficient, in that it requires real-time solving of the differential Riccati equation, and that proofs of global stability can't be given in the general (nonlinear) case. Advances in nonlinear estimation and control techniques have led to the observer presented in [3]. Here, stability guarantees for certain

conditions are given. This observer is further refined by the introduction of road-tire friction adaptation in [4]. The measurement vector used as input consists of lateral and longitudinal acceleration, yaw rate, wheel speed for each wheel and steering angle for each wheel - standard measurements in modern cars with yaw stabilization systems. When making a few, but severely limiting assumptions, such as setting the pitch and roll of the vehicle to zero, the observer is proven to give highly accurate estimates of lateral and longitudinal vehicle velocity. Consequently, safety systems using feedback from these estimates can be expected to function reliably when the car is driven on the highways of continental Europe. However, as e.g. scandinavian drivers are well aware of, the combination of snow and variations in height is quite common; banked, graded and bumpy roads, covered with ice, pose the biggest challenge to the driver and the safety system. It is therefore imparative that the quality of a feedback observer is not too degraded by variations in road structure. This is why it is desired to include GPS velocity in the measurement vector. The idea is that these measurements can be used to compensate for the acceleration measurement error due to vehicle attitude, by helping to identify road grade (RG) and bank angle (RBA) parameters in real-time.

When dealing with measurements, perfection can never be achieved. All signals are approximations to a limited reflection of reality. Still, one has an idea about practical optimality - the concept of removing a problem as cheaply and effectively as possible. Using GPS is most likely not an optimal solution yet. Therefore the problems related to RBA should be evaluated from a more basic perspective, using a roll rate gyro as the only augmentation to the measurement vector. If this proves feasible, it can perhaps fit into the category of practically optimal solutions.

This report deals with key aspects of integrating GPS velocity measurements with the existing nonlinear observer, and development of a gyro based RBA observer. Firstly, the various techniques used for velocity determination by GPS is presented. It is generally not advised to infer velocity information by differentiation of raw position data, but since positioning is the common denominator of all GPS receivers and low cost is a demand, it is highly desirable to see what can be gained by this direct approach. Secondly, limitations and potentials of the observers are discussed, together with ideas on how GPS velocity can be used to improve existing estimates. Finally, results based on simulations and data from a test vehicle are presented.

1.1 Previous work

Integration of GPS and estimation schemes has been done for a wide range of applications and control purposes. In [5], wheel slip, body sideslip angle and tire sideslip angle are estimated using GPS velocity information in conjunction with other sensors. [6] suggests a method for integrating Inertial Navigation System (INS) sensors with GPS measurements to estimate sideslip and cornering stiffness, while [7] focuses on measurement limitations due to noise. In [8], feasibility of controlling a vehicle using GPS-based slip angle measurements is shown. The commonly adopted technique of

correcting inertial sensor errors by use of GPS is described in [9]. All of the above utilize the familiar Kalman filter scheme to state estimation. An ideal approach to pitch and roll estimation, using a two-antenna GPS system, is presented in [10]. Dynamic estimation of RBA, using measurements of lateral acceleration and yaw rate, is shown to be robust for a bicycle model in [11]. Estimation of vehicle parameters, such as mass, rolling resistance and aerodynamic drag, by determining road grade through GPS measurements is demonstrated in [12].

1.2 Nomenclature

CG	- center of gravity of the vehicle
RC	- roll center of the vehicle
PC	- pitch center of vehicle
x_{CG}, y_{CG}, z_{CG}	- axes of the body-fixed coordinate system
n, e, d	- axes of the north-east-down coordinate system
v_x	- vehicle velocity along x_{CG}, longitudinal velocity
v_y	- vehicle velocity along y_{CG}, lateral velocity
v_z	- vehicle velocity along z_{CG}, vertical velocity
ϕ, θ, ψ	- Euler angles (roll, pitch, yaw)
v_x^{CORR}	- actual longitudinal velocity, measured
v_y^{CORR}	- actual lateral velocity, measured
v_x^{GPS}	- GPS-based longitudinal velocity, measured
v_y^{GPS}	- GPS-based lateral velocity, measured
a_x	- longitudinal acceleration, *measured*
a_y	- lateral acceleration, *measured*
r_d	- yaw rate, angular velocity about z_{CG}, *measured*
p_d, q_d	- pitch rate and roll rate relative to the road, *measured* (conditional)
ω_i	- wheel angular velocities, ($i = 1, ..., 4$), *measured*
δ_i	- wheel angles, calculated from steering wheel angle, ($i = 1, ..., 4$)
$\mathbf{d}$	- vector of variables used in the friction model
$\mathbf{g}_i$	- distance vectors from CG to each wheel, ($i = 1, ..., 4$)
μ_H	- maximum road-tire friction coefficient
$\mathbf{F}_i(\mathbf{d}, v_x, v_y, r, \mu_H)$	- friction functions for each wheel, ($i = 1, ..., 4$)
$F_{Z_{ij}}$	- normal force for each wheel, ($ij = FL, FR, RL, RR$)
$R(\delta_i)$	- rotation matrices, wheel-fixed to body-fixed
f_x	- generalized force on the vehicle along x_{CG}
f_y	- generalized force on the vehicle along y_{CG}
f_r	- generalized torque about z_{CG}

J_x, J_y, J_z	- moment of inertia about x_{CG}, y_{CG} and z_{CG} axes
b_F, b_R	- distance between wheeels on front axle/rear axle
l_F, l_R	- distance from CG to front axle/rear axle
h_{CG}	- height of CG
$\Delta h_r, \Delta h_p$	- distance between roll/pitch center and center of gravity
g	- gravitational constant, 9.81 m/s

Chapter 2

Vehicle model

The vehicle model in Figure 2.1 is the same as in [3, 4].

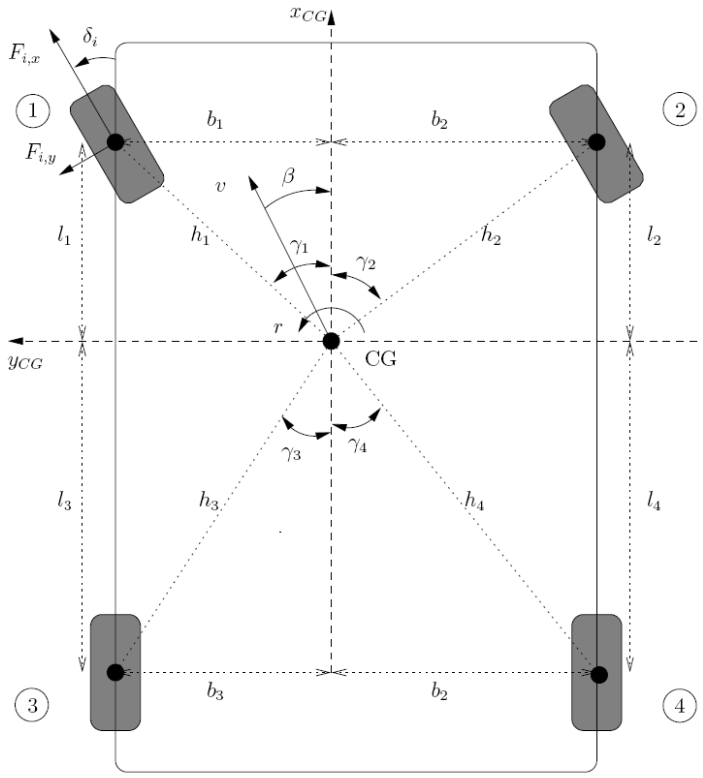

Figure 2.1: Vehicle model

In [3], only forces caused by road-tire friction are included. This means that e.g. air resistance is ignored in the dynamic equations. To compute the friction forces, a nonlinear friction model is used. Generalized resultant forces are defined as

$$f_x(t, v_x, v_y, r) := \sum_{i=1}^{4} [1\ 0] R(\delta_i) \mathbf{F}_i(\mathbf{d}, v_x, v_y, r, \mu_H) \tag{2.1}$$

$$f_y(t, v_x, v_y, r) := \sum_{i=1}^{4} [0\ 1] R(\delta_i) \mathbf{F}_i(\mathbf{d}, v_x, v_y, r, \mu_H) \tag{2.2}$$

$$f_r(t, v_x, v_y, r) := \sum_{i=1}^{4} [0\ 1] \mathbf{g}_i^T R(\delta_i) \mathbf{F}_i(\mathbf{d}, v_x, v_y, r, \mu_H) \tag{2.3}$$

The resulting equations of motion are

$$\dot{v}_x = a_x + r v_y \tag{2.4}$$

$$\dot{v}_y = a_y - r v_x \tag{2.5}$$

$$\dot{r}_r = \frac{1}{J_z} f_r(t, v_x, v_y, r) \tag{2.6}$$

It can immediately be seen that this model does not include information about dynamics along the z-axis. This is because roll and pitch of the vehicle have been ignored in the existing observer scheme. Since vehicle attitude has a direct influence on acceleration measurements, it is desirable to augment the existing model so that observability of this coupling is increased. Figure 2.2, which is slightly modified from [13], illustrates how the combination of road structure and driving pattern affects attitude of the vehicle body. Note that two coordinate frames are defined for the vehicle - road frame and dynamic frame. The xy-plane of the road frame is parallel to the imaginary plane defined by the contact points between wheels and road. The dynamic frame is rotated from the road frame by the angles ϕ_v and θ_v. Both have origins in the CG.

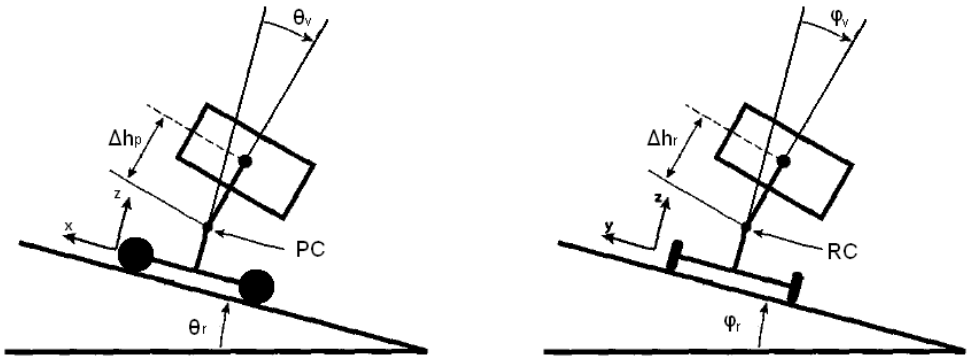

(a) Pitch (b) Roll

Figure 2.2: Vehicle pitch and roll

ECEF position	$\mathbf{p}^e = \begin{bmatrix} x_e \\ y_e \\ z_e \end{bmatrix} \in \mathbb{R}^3$	Longitude and latitude	$\mathbf{\Psi} = \begin{bmatrix} l \\ \mu \end{bmatrix} \in \mathcal{S}^2$
NED position	$\mathbf{p}^n = \begin{bmatrix} n \\ e \\ d \end{bmatrix} \in \mathbb{R}^3$	Attitude (euler angles)	$\mathbf{\Theta} = \begin{bmatrix} \phi \\ \theta \\ \psi \end{bmatrix} \in \mathcal{S}^3$
Body-fixed linear velocity	$\mathbf{v}_o^b = \begin{bmatrix} u \\ v \\ w \end{bmatrix} \in \mathbb{R}^3$	Body-fixed angular velocity	$\boldsymbol{\omega}_{nb}^b = \begin{bmatrix} p_b \\ q_b \\ r_b \end{bmatrix} \in \mathbb{R}^3$

Table 2.1: Frame associated vectors

$\mathbb{R}^n$ is the *Euclidian space* of dimension n and $\mathcal{S}^n$ denotes a *torus* of dimension n.

For the idea of vehicle roll and pitch angle to give meaning, the body-fixed coordinates must be related to another frame. Here, this is the North-East-Down (NED) frame. NED is the tangent plane on the surface of the earth, moving with the vessel [14], where the axes n, e and d point towards north, east and the center of the earth respectively. It is important to note that directions of the n and e axes are not dependent on the orientation of the vehicle; they simply define a virtual plane which allows definition of relative vehicle orientation. Attitude is given as angles between body-fixed (road) and NED coordinate axes. These are referred to as the *Euler angles* [15].

ψ - rotation about the z_1 axis
θ - rotation about the current (rotated) y axis
ϕ - rotation about the current (rotated) x axis

Equations 2.4-2.5 are based on the assumption that ϕ and θ are both zero. If they are not, the acceleration measurements a_y and a_x will be biased by gravitational components given as w_ϕ and w_θ. To determine the magnitude of these biases, kinematic relations are used. It is necessary to rotate the gravitational vector in the inertial frame to the body fixed frame. The x and y components of the rotated vector represent acceleration biases due to vehicle attitude. Using notation from Table 2.1, the following expressions are derived

$$\begin{aligned}\mathbf{g}^n &= \begin{bmatrix} 0 & 0 & g \end{bmatrix}^T \\ \mathbf{g}^b &= \mathbf{R}_b^n(\mathbf{\Theta})^T \mathbf{g}^n \\ w_\theta &= \mathbf{e}_x^T \mathbf{g}^b \\ w_\phi &= \mathbf{e}_y^T \mathbf{g}^b\end{aligned}$$

Where $\mathbf{R}_b^n(\mathbf{\Theta})$ is a rotation matrix defined as

$$\mathbf{R}_b^n(\mathbf{\Theta}) = \begin{bmatrix} \cos\psi\cos\theta & -\sin\psi\cos\phi + \cos\psi\sin\theta\sin\phi & \sin\psi\sin\phi + \cos\psi\cos\phi\sin\theta \\ \sin\psi\cos\theta & \cos\psi\cos\theta + \sin\phi\sin\theta\sin\psi & -\cos\psi\sin\phi + \sin\theta\sin\psi\cos\phi \\ -\sin\theta & \cos\theta\sin\phi & \cos\theta\cos\phi \end{bmatrix}$$

resulting in the expressions

$$\begin{aligned}w_\theta &= -g\sin\theta \\ w_\phi &= g\cos\theta\sin\phi\end{aligned}$$

Properties of the rotation matrix **R** are described in Appendix A.1. The simplest way to find the Euler angles, is to use a two-antenna GPS system, but this is currently not an option. It will be necessary to estimate θ and ϕ using available sensors. To achieve this, kinematic properties of the sensors have to be known.

Assumption 2.1: Sensors a_x, a_y, and r_d, are located at the center of gravity.

Assumption 2.2: If pitch rate and roll rate sensors are available, they are denoted p_d and q_d.

Assumption 2.3: All wheels are in contact with the ground at all times.

Angular velocities in the road frame must be converted by means of a transformation matrix before a meaningful integration can be performed. Table 2.1 defines the body fixed angular velocity vector $\boldsymbol{\omega}_{nb}^b$. Since the vehicle body is expressed in terms of two body fixed coordinate systems, it is necessary to separate these two. Angular velocity in the road frame is given as $\boldsymbol{\omega}_{nr}^r$, while angular velocity in the dynamic frame is given as $\boldsymbol{\omega}_{nd}^d$. According to [14], the relationship is expressed as

$$\boldsymbol{T}_{\boldsymbol{\Theta}} = \begin{bmatrix} 1 & \sin\phi\tan\theta & \cos\phi\tan\theta \\ 0 & \cos\phi & -\sin\phi \\ 0 & \frac{\sin\phi}{\cos\theta} & \frac{\cos\phi}{\cos\theta} \end{bmatrix}$$

$$\dot{\boldsymbol{\Theta}} = \boldsymbol{T}_{\boldsymbol{\Theta}}(\boldsymbol{\Theta})\boldsymbol{\omega}_{nr}^{r} \tag{2.7}$$

Now, the Euler rates for can be written out in component form

$$\dot{\phi} = p_r + q_r \sin\phi\tan\theta + r_r \cos\phi\tan\theta \tag{2.8}$$
$$\dot{\theta} = q_r \cos\phi - r_r \sin\phi \tag{2.9}$$
$$\dot{\psi} = q_r \frac{\sin\phi}{\cos\theta} + r_r \frac{\cos\phi}{\cos\theta}, \theta \neq \pm\frac{\pi}{2} \tag{2.10}$$

It is necessary to find the relationship between derivatives of road bank angle and road grade, and the Euler angles. Firstly, it should be stated that ϕ_r and θ_r are physically decoupled from the vehicle, although they are fully dependent on vehicle position and orientation. Secondly, the Euler angles represent orientation of the road frame, not the dynamic frame, which means that ϕ and θ depend fully on ϕ_r and θ_r. Yaw is insignificant with regards to road bank angle and road grade. By recalling that Euler angle θ is a rotation about current y-axis, it is obvious that θ_r equals θ. Since ϕ is rotation about current x-axis, θ affects ϕ. The rate expressions become

$$\dot{\phi}_r = \cos\theta\dot{\phi} \tag{2.11}$$
$$\dot{\theta}_r = \dot{\theta} \tag{2.12}$$

By substitution of equations 2.8-2.9

$$\dot{\phi}_r = p_r \cos\theta + q_r \sin\phi\sin\theta + r_r \cos\phi\sin\theta \tag{2.13}$$
$$\dot{\theta}_r = q_r \cos\phi - r_r \sin\phi \tag{2.14}$$

Rotation between the road frame and the dynamic frame

$$\mathbf{R}_r^d(\boldsymbol{\Theta}_\mathbf{v}) = \mathbf{R}_{x,\phi_v}^T \mathbf{R}_{y,\theta_v}^T = \begin{bmatrix} \cos\theta_v & 0 & -\sin\theta_v \\ \sin\theta_v\sin\phi_v & \cos\phi_v & \cos\theta_v\sin\phi_v \\ \sin\theta_v\cos\phi_v & -\sin\phi_v & \cos\theta_v\cos\phi_v \end{bmatrix} \tag{2.15}$$

Now, the measurements of rotation can be expressed as functions of kinematic variables.

$$\boldsymbol{\omega}_{nd}^{d} = \begin{bmatrix} \dot{\phi}_v \\ \dot{\theta}_v \\ 0 \end{bmatrix} + \mathbf{R}_r^d(\boldsymbol{\Theta}_\mathbf{v})\boldsymbol{\omega}_{nr}^r \tag{2.16}$$

In component form:

$$p_d = p_r \cos\theta_v - r_r \sin\theta_v + \dot{\phi}_v \tag{2.17}$$
$$q_d = p_r \sin\theta_v \sin\phi_v + q_r \cos\phi_v + r_r \cos\theta_v \sin\phi_v + \dot{\theta}_v \tag{2.18}$$
$$r_d = p_r \sin\theta_v \cos\phi_v - q_r \sin\phi_v + r_r \cos\theta_v \cos\phi_v \tag{2.19}$$

Ideally, a complete dynamic model of vehicle roll and pitch should be developed, but due to the simplicity of the underlying goal, which is robust estimation of v_y, and the small number of sensors, focusing on roll alone is a more feasible approach. This means that a few assumptions have to be made.

Assumption 2.4: Pitch angle $\theta = 0$.

Now equations 2.17 and 2.19 become

$$p_d = p_r + \dot{\phi}_v \approx \dot{\phi}_r + \dot{\phi}_v \tag{2.20}$$
$$r_d = r_r \cos\phi_v - q_r \sin\phi_v \tag{2.21}$$

The point to be illustrated with these kinematic relations, is that a roll rate measurement, in this case p_d, is only an approximation to a linear superposition of $\dot{\phi}_v$ and $\dot{\phi}_r$, meaning that the useful information is hard to extract. It is impossible to measure bank angle (semi) directly without a two-antenna GPS configuration; even with an angular velocity gyro measurement, bank angle information will in some cases be completely invisible in the sensor data. This is the case when the vehicle performs a circle maneuver on a large, tilted plane. Therefore one can assume that a simple sensor configuration will be inadequate in terms of exact bank angle determination. However, it is possible that improvements in the velocity estimation can be made by accounting for errors due to vehicle roll. A model of vehicle roll must be developed.

For convenience, the two-track model presented in [16] will be used here as well. Figure 2.3 illustrates the basic mass-spring-damper characteristics of the system. The original expression is

$$\ddot{\phi}_v = \frac{1}{J_x}[f_y h \cos\phi + mgh \sin\phi - C_\phi \phi - K_\phi \dot{\phi} + \dot{\psi}^2 (J_y - J_z) \sin\phi \cos\phi]$$

The modeled quantity is obviously ϕ_v, not ϕ_r. Intuitively, ϕ_v should be fairly small, since there are physical limitations to how much the springs can be compressed. This means that the model can be simplified in terms of trigonometry, resulting in the following equation

$$\ddot{\phi}_v = \frac{1}{J_x}[f_y h + mgh\phi - C_\phi \phi - K_\phi \dot{\phi} + \dot{\psi}^2 (J_y - J_z)\phi]$$

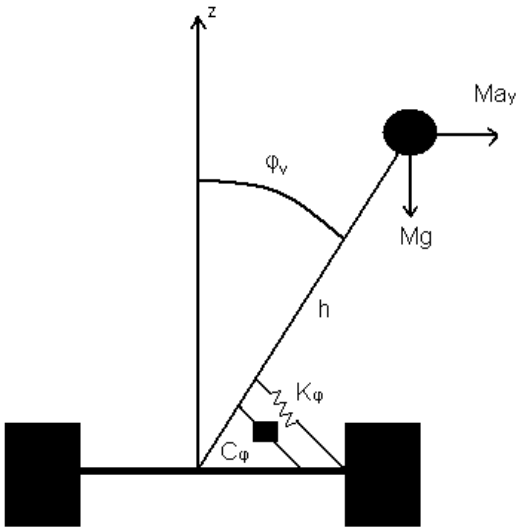

Figure 2.3: Roll dynamics

Parameters K_ϕ and C_ϕ depend on the spring-damper configuration, but will have values that help force ϕ_v to zero. $\dot{\psi}$ is assumed equal to the yaw rate measurement r. The new set of differential equations becomes

$$\dot{v}_x = a_x + r v_y - w_\theta = a_x + r v_y + g \sin\theta \tag{2.22}$$

$$\dot{v}_y = a_y - r v_x - w_\phi = a_y - r v_x - g \cos\theta \sin\phi \tag{2.23}$$

$$\dot{r} = \frac{1}{J_z} f_r(t, v_x, v_y, r) \tag{2.24}$$

$$\ddot{\phi}_v = \frac{1}{J_x}[f_y(t, v_x, v_y, r)h + mgh\phi - C_\phi \phi - K_\phi \dot{\phi} + r h^2 (J_y - J_z)\phi] \tag{2.25}$$

Notice that there is no link between ϕ and ϕ_v at this point. This link will have to be established in conjunction with the development of a state estimator.

Chapter 3

GPS

Two definitions of GPS are presented. “GPS is an all-weather, worldwide, continuous coverage, satellite-based radio-navigation system” [17] and “The NAVSTAR Global Positioning System (GPS) is a satellite-based radio-positioning and timetransfer system designed, financed, deployed, and operated by the U.S. Department of Defense” [18]. Currently, applications range from handheld devices that can be used for positioning by the general public, to dynamic positioning and navigation of large vessels, such as ships and airplanes.

The automotive industry and its suppliers have realized the potential of integrating this technology with multimedia solutions to give drivers and passengers the ability to navigate effortlessly through the aid of digital maps. This is by no means standard equipment for low-priced cars, but hints at future solutions where less time is spent on finding the way, and more time on performing the safety critical tasks presented to the driver. As GPS equipment becomes cheaper and safety demands increase, it is interesting to find new areas of application. In light of this, knowing the basic modes of operation is key to understanding limitations and potentials of new solutions. The following sections describe positioning and velocity determination by GPS, largely based on [17].

3.1 Positioning

Position determination using GPS is a complex process where several mathematical techniques can be applied. Different manufactures use different approaches, which gives a large variety in price and quality of the end product As this report focuses on use of existing solutions, quantitative aspects and receiver implementations will not be covered. Fundamentals of GPS positioning are briefly evaluated in a qualitative manner. GPS is described in terms of segments: The space segment, the control segment and the user segment.

The space segment

Using an informal comparison, the space segment is reminiscent of the physical layer in the International Standard Organization's Open System Interconnect (ISO/OSI) network model: It consists of the GPS satellites orbiting the earth. Currently, 30 Block II/IIA/IIR/IIR-M satellites are operational. For a detailed description, see [19].

GPS satellites orbit the earth in semi-circular orbital planes, with a configuration that ensures visibilty of five to eight satellites from any point on earth. These orbits are not geoshynchronous, however, making the position-estimation accuracy time-varying for a given set of satellites. This is called Geometric Dilution of Precision (GDOP), which can be kept at a stably low level by changing satellite combinations.

The control segment

This segment monitors health and status of the space segment. Ground monitoring stations measure signals from the satellites, and transmit these to a master control station. The master calculates orbital model and clock correction parameters for each satellite, which receive these updated values from ground antennas.

The user segment

The user segment consists of the multitude of GPS antenna/receiever pairs used for military, industrial and public service purposes. Receivers provide users with position, velocity and timing information, based on signals transmitted by the satellites. No signals are transmitted from receiver to satellite, meaning that the system won't experience increased load when the number of active receivers increases.

3.1.1 Standard positioning

Mode of operation

GPS satellites transmit ranging codes and navigation data by code-division multiple access (CDMA) on two frequencies, L1 (1575.42 MHz) and L2 (1227.60 MHz). These are modulated by spread-spectrum signals to carry information to the user. Each satellite is associated with three pseudorandom noise (PRN) ranging codes. In short, GPS receivers lock on to satellites by correlating internally generated versions of the PRN codes with the ones received from the satellites. Each satellites has a unique code, making cross-satellite interference small.

Position determination is based on the fact that radio signals travel at the speed of light. Receivers note the time of arrival of satellite ranging codes, and use this information to find the propagation time from satellite to receiver. Propagation time multiplied with speed of light equals pseudorange. The reason it is called pseudorange, is that clock errors give a bias to the calculated propagation time. Several techniques for bias compensation exist. For a detailed description, see Chapter 5.4 in [17].

When satellite location is known, the pseudorange measurement defines a sphere of possible receiver locations. An accurate position measurement is given by the intersection of four such spheres. It is possible to use three pseudrorange measurements and a model of the earth as the fourth sphere, but in practice one always has four or more pseudoranges. This leads to a set of nonlinear equations which contain the various bias terms, and GPS receivers adopt extended Kalman filtering techniques to estimate their solutions.

Accuracy

Several forms of error contribute to the deterioration of quality in GPS range measurements, all of which can be categorized as common mode or non-common mode. Common mode errors will be experienced in the samme manner by all GPS receivers in a limited geographic area. Non-common mode errors are specific for given locations and receivers. Typical standard deviations for the various sources of noise are given in Table 3.1

Errors	Standard deviation (m)
Common mode	
Ionosphere	7.0
Clock and ephemeris	3.6
Troposphere	0.7
Noncommon mode	
Receiver noise	0.1-0.7
Multipath	0.1-3.0

Table 3.1: Error due to noise sources

The effect these have on position estimates can be expressed in terms of DOP factors, which are found from the covariance matrix for user position and clock bias errors. This is typically done in real-time software. From the users perspective, knowing how accurate a position measurement generally will be be is usually enough. In situations with low non-common mode error, this number can be approximated to 25 meters [20], meaning that a GPS receiver operating in standard mode will give position information containing an error of 0-25 meters.

3.1.2 Advanced positioning

Several features of GPS can be exploited to give (much) more accurate position estimates. The problem with these improvements is that they must be supported by hardware and external references, making them unsuitable for use with standardized estimation schemes. Also, advanced hardware obviously leads to increased cost. For

these reasons, advanced positioning is only briefly described. Techniques directly related to velocity estimation will be discussed in 3.2.

Differential GPS

Differential GPS (DGPS) is an effective approach to dealing with common mode errors. Since common-mode errors are the same for all receivers in a limited geographic area, they can be reduced if a stationary receiver at a known location (base) estimates them and broadcasts this information to the mobile units, which in turn use this to compensate for errors. This results in accuracies of 1-5 meters. Distance between mobile units and the base should not exceed 100 km, as this reduces correlation of common mode errors.

DGPS is a common option for relatively low-cost receivers, so from an economical perspective, this approach has merit. The main drawback lies in reliance on DGPS base stations. Cars very often don't follow preplanned routes, so availability of base stations is non-deterministic. Therefore, using DGPS becomes an implementation issue. If a vehicle state estimation scheme is to benefit from GPS measurements, it must be able to determine what accuracy can be expected from the GPS receiver. In short, measurements with high accuracy should be used when available, but the main concern is that the estimation scheme works for low-level operating conditions. Possible improvements due to DGPS can be investigated in future work.

Two-Frequency receivers

Two-frequency receivers use pseudorange measurements from two different frequency bands to estimate ionospheric delays. Low-pass filtering the estimated delay and subtracting it from the pseudorange gives increased accuracy of position estimates. The practical drawback is that the receiver needs to support two frequencies.

Carrier phase tracking

Carrier phase tracking is based on the idea that phase shifts in the carrier can be tracked if the receiver phase locks to the carrier signal. The number of carrier cycles between a receiver and a satellite can't be measured directly, but the change in number of cycles, however, can be measured. Motivation for determining the carrier phase observable stems from the fact that it reduces non-common mode errors by an approximate factor of 0.01. To be able to use the carrier phase observable, a number called the integer phase ambiguity has to be estimated. This is the whole number of carrier phase cycles between the receiver and the satellite at an initial measurement time. Resolving the integer ambiguity is a non-trivial matter, and several approaches exist. See [21, 22, 23].

Carrier phase aided positioning requires use of a DGPS scheme, or else the integer ambiguity can't be computed. As discussed, this is currently not viable for use in a general purpose safety system.

3.2 Velocity determination

There are two main approaches to velocity determination using GPS: time differentiation of position measurements, and doppler carrier phase processing. Advantages and disadvantages of the two approaches are discussed in the following sections. Note that the variables used are discrete for real-time applications. This means that any GPS measurement, denoted X, will actually be the value of X_k at sample time k. Consequently, $\dot{X}$ refers to the discrete derivative, given as

$$\dot{X} = \frac{X_k - X_{k-1}}{\frac{1}{\epsilon}}$$

where ϵ is the sampling frequency. The receiver used in the tests referred to in this report, has $\epsilon = 10$ Hz.

3.2.1 Differentiating position measurements

Using dynamic position measurements to derive velocity is intuitively appealing, as the physical interpretation of velocity is change in position with respect to time. Since virtually all GPS receivers present position data to the user, a receiver independent velocity estimation scheme can be implemented. Key aspects are position representation, kinematics and noise handling.

Position measurements only make sense with relation to a geometric reference frame. Terrestrial navigation usually doesn't involve more than three standarized frames: Earth-centered Earth-fixed (ECEF), North-East-Down (NED) and BODY. These are described in [14]. Vectors associated with each frame are defined in Table 2.1.

Standard receiver output is longitude and latitude Ψ, and height above mean sea level (MSL) h. These values are useful in map-based navigation, but need to be transformed for effective computation of secondary information, such as velocity. GPS systems use a reference ellipsoid, WGS-84, which relates ECEF coordinates to longitude and latitude. Calculation of ECEF position from longitude, latitude and height is given by:

$$\mathbf{p}^e = \begin{bmatrix} x_e \\ y_e \\ z_e \end{bmatrix} = \begin{bmatrix} (N+h)\cos\mu\cos l \\ (N+h)\cos\mu\sin l \\ (\frac{r_p^2}{r_e^2}N + h)\sin\mu \end{bmatrix} \tag{3.1}$$

$$N = \frac{r_e^2}{\sqrt{r_e^2\cos^2\mu + r_p^2\sin^2\mu}}$$

$$r_e = 6378137m$$

$$r_p = 6356752m$$

where N is the radius of curvature in the prime vertical and r_e and r_p are WGS-84 parameters. The set of ECEF coordinates in $\mathbf{p}^e$ will be considered measured variables in the following sections, since equation 3.1 is a static transformation, and direct time-differentiation of computed $\mathbf{p}^e$ gives the same result as time-differentiation of the analytical expressions of x_e, y_e and z_e.

Kinematics

The position vector $\mathbf{p}^e$ represents distances along three earth fixed axes defined as the (accelerated) ECEF frame. Its derivative, $\dot{\mathbf{p}}^e$, consequently only gives information about the positional change of a point in space, relative to the center of the earth, with regards to time. This has limited usefulness in practical applications, so $\dot{\mathbf{p}}^e$ needs to be converted by means of kinematic manipulation. To decide what transformations should be made, one has to look at the task to be performed. When dealing with ground based vehicles, the NED and BODY frames give intuitive representations of linear velocity, angular velocity and attitude. Linear velocity $\mathbf{v}_o^b$ of the GPS receiver, given in the BODY frame, is the velocity the receiver has along its x_b, y_b and z_b axes, where the origin lies at the base of the receiver. Ideally, the u and v components of $\mathbf{v}_o^b$ should be equal to the correct values of v_x and v_y of the vehicle the receiver is associated with, but this will generally not be the case. For this reason, $\mathbf{v}_o^b$ will be referred to as receiver velocity instead of vehicle velocity. Finding $\mathbf{v}_o^b$ is done using the following relation:

$$\dot{\mathbf{p}}^e = \mathbf{R}_n^e(\Psi)\mathbf{p}^n = \mathbf{R}_n^e(\Psi)\mathbf{R}_b^n(\Theta)\mathbf{v}_o^b \tag{3.2}$$

Premultiplying with the transpose of the rotation matrices gives

$$\mathbf{v}_o^b = \mathbf{R}_b^n(\Theta)^T\mathbf{R}_n^e(\Psi)^T\dot{\mathbf{p}}^e \tag{3.3}$$

where $\mathbf{R}_n^e(\Psi)$ is defined as

$$\mathbf{R}_n^e(\Psi) = \begin{bmatrix} -\cos l \sin\mu & -\sin l & -\cos l\cos\mu \\ -\sin l\sin\mu & \cos l & -\sin l\cos\mu \\ \cos\mu & 0 & -\sin\mu \end{bmatrix}$$

From 3.3 it can be seen that the receiver's linear velocity is related to the differentiated position measurements through the attitude (Euler angle) vector Θ, which is the argument of $\mathbf{R}_b^n$. Ideally one would have measurements or estimates of all three angles, but in the current configuration, none are available. The first step in circumventing this problem, is to assume that roll ϕ and pitch θ of the vehicle are both zero. Considering that RBA and RG give the vehicle roll and pitch, this assumption can appear counterproductive. However, ignoring RBA and RG when calculating $\mathbf{v}_o^b$, leads to the possibility of finding attitude information from the difference in observer based velocity and GPS based velocity.

If 3.3 is to make sense, a good measurement of ψ is needed. Since the orientation of the receiver is static with regards to the orientation of the vehicle, ψ can be defined as equal for both. From a mathematical point of view, it would seem logical to perform an integration of the yaw-rate measurement r, but two things stand in the way of this approach. Integrating the biased yaw-rate gyro measurement gives large offsets over time. It is also impossible to know the initial yaw of the vehicle. Because of this, ψ can't be determined accurately. A new assumption is needed. When sideslip is low, the absolute velocity can be assumed to point in nearly the same direction as longitudinal velocity v_x of the vehicle. The direction of absolute velocity is called course. Let absolute velocity and course in the two dimensional NE-frame be defined as V and ψ_c, where

$$V := \sqrt{\dot{n}^2 + \dot{e}^2} \tag{3.4}$$

$$\psi_c := Atan2(\dot{n}, \dot{e}) \tag{3.5}$$

From 3.5 it can be seen that the velocity components $\dot{n}$ and $\dot{e}$ must be calculated. They are found as the the first two elements of $\dot{\mathbf{p}}^n$, given

$$\dot{\mathbf{p}}^n = \mathbf{R}_n^e(\Psi)^T \dot{\mathbf{p}}^e \tag{3.6}$$

Substituting Θ in $\mathbf{R}_b^n(\Theta)$ with Θ_c, where

$$\Theta_c := \begin{bmatrix} 0 \\ 0 \\ \psi_c \end{bmatrix} \tag{3.7}$$

gives

$$\mathbf{R}_b^n(\Theta_c) = \begin{bmatrix} \cos\psi_c & -\sin\psi_c & 0 \\ \sin\psi_c & \cos\psi_c & 0 \\ 0 & 0 & 1 \end{bmatrix} \tag{3.8}$$

For ease of distinction, $\mathbf{v}^{GPS}$ is defined

$$\mathbf{v}^{GPS} := \begin{bmatrix} v_x^{GPS} \\ v_y^{GPS} \\ v_z^{GPS} \end{bmatrix} = \mathbf{v}_o^b \tag{3.9}$$

Substituting 3.8 and 3.9 into 3.3, gives

$$\mathbf{v}^{GPS} = \mathbf{R}_b^n(\Theta_c)^T \mathbf{R}_n^e(\Psi)^T \dot{\mathbf{p}}^e \tag{3.10}$$

This simple expression determines receiver velocity in the BODY frame, by transformation of measured receiver position in the ECEF frame.

Noise and filtering

GPS accuracy determination is a field of study which requires rigorous and time consuming test procedures, combined with statistical methods. This report focuses on relevance and feasibility of integrating existing GPS solutions with a nonlinear observer, and consequently a detailed analysis of the accuracy of the receiver used in the tests presented, is not given. Here it is more interesting to see what can be gained by using a general class receiver in a direct manner.

If $\mathbf{p}^e$ was a perfect measurement, direct calculation of 3.10 would give a perfect estimate of the receiver's linear velocity when moving in a horizontal plane, without difference between yaw and course. To no great surprise, this generally does not hold. Firstly, position measurements have time correlated errors. In practice, this means that a north-east position plot for a static receiver, taken over time, will give a "wandering" graph contained within a circular region, disregarding error-spikes due to multipath or signal loss. The structure of the time correlation cannot be determined without access to internal receiver variables. On a positive note, the position error is slowly varying. If the position error jumped between e.g. -10 m and 10 m for two consecutive samples, with frequency 10 Hz, a differentiation of the measurement would give an instantaneous absolute velocity of 200 m/s, which of course would render the differentiation useless. To illustrate how the position measurement error varies, Figure 3.1(a) shows a plot of the *Euclidian norm* of the normalized ECEF position vector, $\|\mathbf{p}^e\|_2$, with zero mean, for a static receiver sampling at 10 Hz. The actual value of the position measurement is unimportant, but how it varies around the mean, or correct value, is not. 3.1(b) gives an idea of what velocity errors can be expected when purely differentiating the unfiltered position measurements. For this particular set of data, the maximum value of velocity error is approximately 0.4 m/s, or 1.44 km/h. To put this into perspective: The position measurement error can be significant if used to estimate low velocities, such as v_y.

When the receiver is accelerated (within the ECEF frame), error magnitude increases. This is harder to analyze, since the receiver's actual trajectory isn't known. It is, however, possible to compare measured position trajectories with corresponding velocity trajectories, and try to infer noise information from this. Figure 3.2 shows a normalized trajectory of y_e alongside $\dot{y}_e$, for a flat surface vehicle test with slalom maneuver. Note that similar results are obtained for x_e and z_e. The shape of $\dot{y}_e$ is in no way subtle - direct differentiation gives huge, noise-like spikes in calculated velocity. Through closer inspection, it is revealed that the noise is caused by something similar to quantization error in the position measurement. When two consecutive samples have the same value, the time derivative approaches zero. From the shape of 3.2(a), it can be

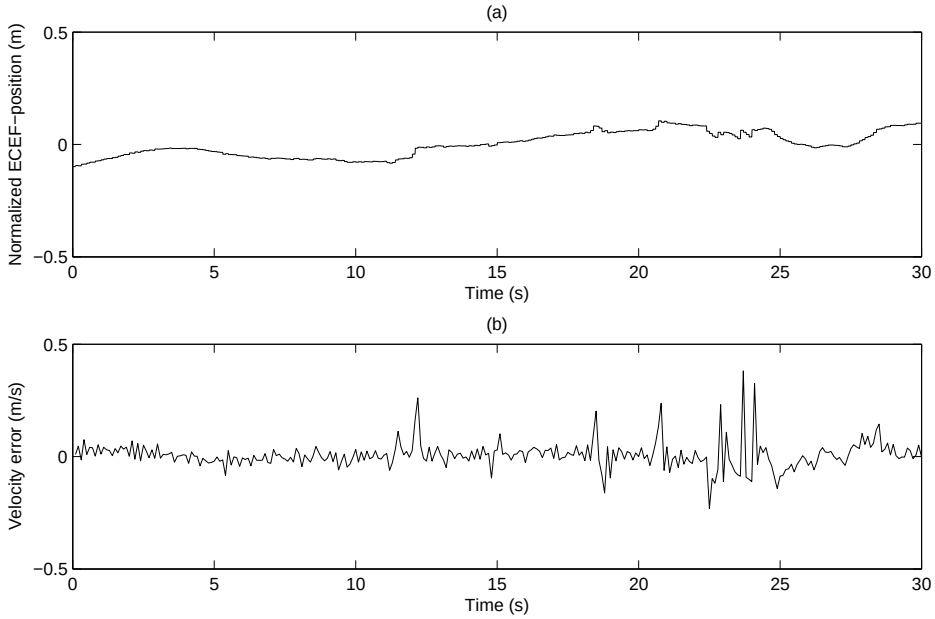

Figure 3.1: (a) Variations in absolute ECEF position about mean value for a static receiver. (b) Velocity error due to position error

seen that the vehicle *most likely* undergoes continuous motion, so existence two identical consecutive samples must be caused by an error in the GPS signal or receiver algorithm.

The problem illustrated by Figure 3.2, has to be accounted for. In this report, three approaches are considered:

Method 1: Linear filtering of the time differentiated 10Hz position measurement.

To utilize a linear filter efficiently, it is important to know the frequency properties of the signal. The goal is to filter out high-frequency noise components, without affecting signal information too much. A typical approach to decoupling noise and signal, is to subtract a perfect measurement from the noisy one, leaving a noise sequence with base at zero. For ease of implementation, $\mathbf{v}^{GPS}$ will be used instead of $\dot{\mathbf{p}}^e$, even though this means that the errors in the measurement-dependent rotation matrices will contribute to the end-signal error. The nonlinear observer from [3] will be considered a "perfect" measurement. In short, this is the only way of comparison currently available. A detailed description of digital signal processing can be found in [24].

The first step is to determine the power spectral density (PSD), denoted $S(\omega)$, of the signal noise. This gives information about which frequency bands have to be filtered. To find the PSD, numerical methods are applied to the noise sequence. See Appendix

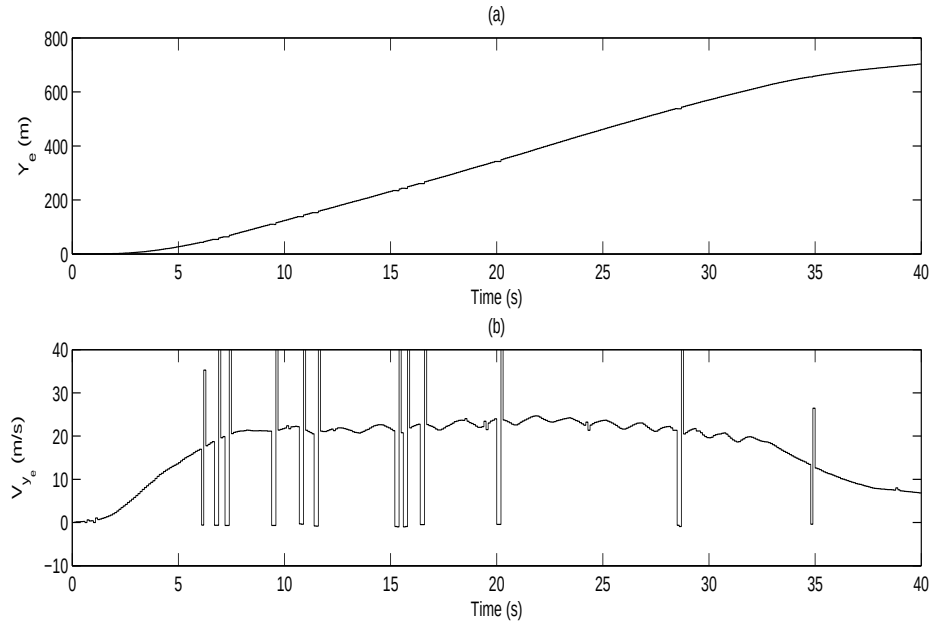

Figure 3.2: (a) y_e (b) $\dot{y}_e$

B.2 for details. Figure 3.3 shows noise sequence and PSD for longitudinal velocity, given by the same test as in Figure 3.2. It can bee seen that most of the noise power lies from about 1 Hz and up. This knowledge will be used to synthesize a discrete low-pass filter.

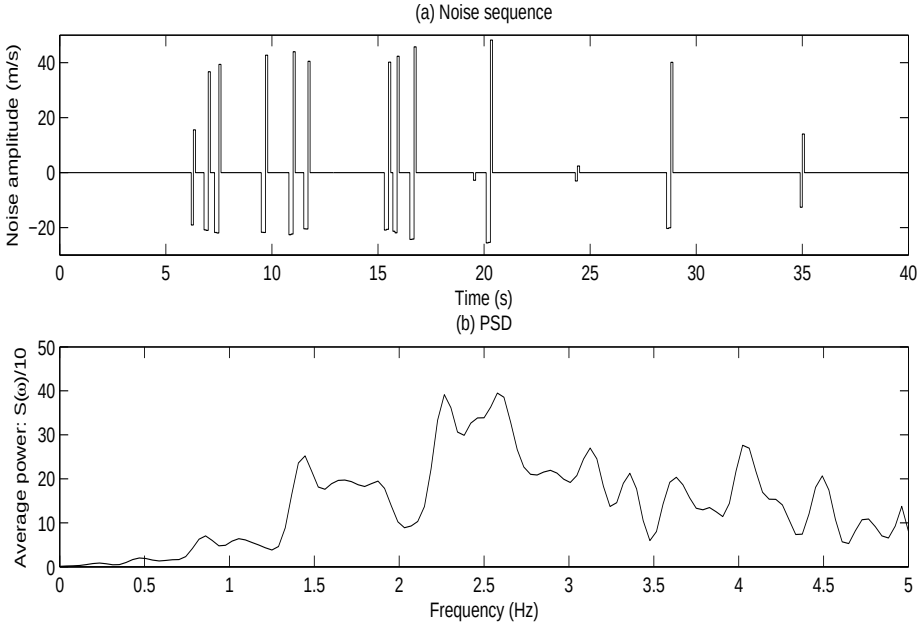

Figure 3.3: (a) Noise sequence extracted from v_x^{GPS} (b) PSD of the noise sequence

The filter is presented as a transfer function in the complex z-domain, and takes the following generalized form:

$$H(z) = \frac{B(z)}{A(z)} = \frac{b_1 + b_2 z^{-1} + \cdots + b_{n+1} z^{-n}}{1 + a_2 z^{-1} + \cdots + a_{n+1} z^{-1}} \tag{3.11}$$

n denotes the filter order, and a and b are filter coefficients. This configuration gives a *Butterworth filter*. Desired low-pass characteristics are determined by n, a and b, which are user-specified parameters. By making appropriate choices, the *cutoff frequency* ω_c, defined here as

$$\omega_c \Rightarrow |H(\omega_c)| = \frac{1}{\sqrt{2}} \tag{3.12}$$

can be placed in such a way that undesired high-frequency components are damped. By recalling that the noise sequence had most of its power in the frequency range above 1 Hz, the following statement can be made:

$$\omega_c \leq 1 \text{ Hz}$$

The reason ω_c isn't more accurately specified, is that one usually has to try several configurations before good filtering is achieved. Determining a and b is most easily done by using the MATLAB function *butter()*, which is described in Appendix B.1.

Phase delay is the main drawback when using linear filters in real-time applications. If a signal is to be used in a feedback loop, a delay of just a few milliseconds can render it useless. Therefore, a compromise between smoothing and delay must be made. Through experimentation, it is discovered that even a low-order-high-cutoff filter gives the signal a significant phase delay. Figure 3.4 shows comparisons between the filtered GPS signals and actual vehicle velocities. In this case, noise has been adequately damped, but it's obvious that the phase delay is too great for the signal to be of use. By reducing filter order and increasing ω_c, noise becomes the dominating factor in signal degradation. It is possible to conclude that low-pass filtering the differentiated signal is not a feasible approach to dealing with noise.

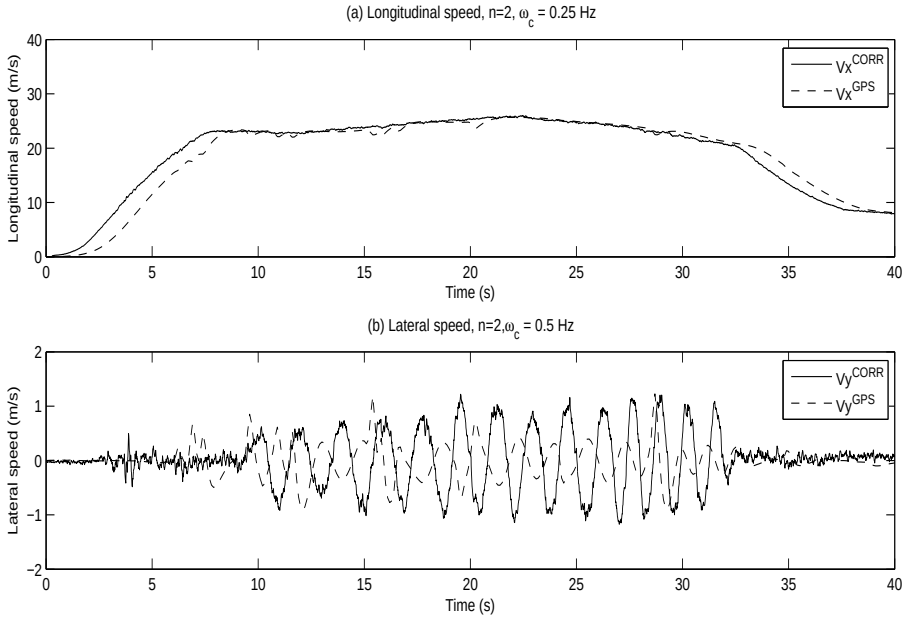

Figure 3.4: (a) Actual v_x and filtered v_x^{GPS} (b) Actual v_y and filtered v_y^{GPS}

Method 2: Resampling the position measurement at 100Hz, smoothing the new signal with a linear filter, downsampling to 10Hz, time differentiating the smooth 10Hz signal.

The idea here is that the measurement signal can be smoothed by means of sampling and filtering. By upsampling the GPS signal to 100Hz, no information is gained or lost. Filtering the new signal with a cut-off frequency of about 10Hz should result in a smoother version of the original signal. Downsampling this to 10Hz gives a signal with fewer "flat spots" than the original signal, and consequently a better candidate for differentiation.

This procedure uses the same filter structure as in **Method 1**, so the best results are presented directly. See Figure 3.5. Note that it's the ECEF position signals that are filtered. Without providing any further discussion, it is stated that **Method 2** is infeasible for this type of filtering problem.

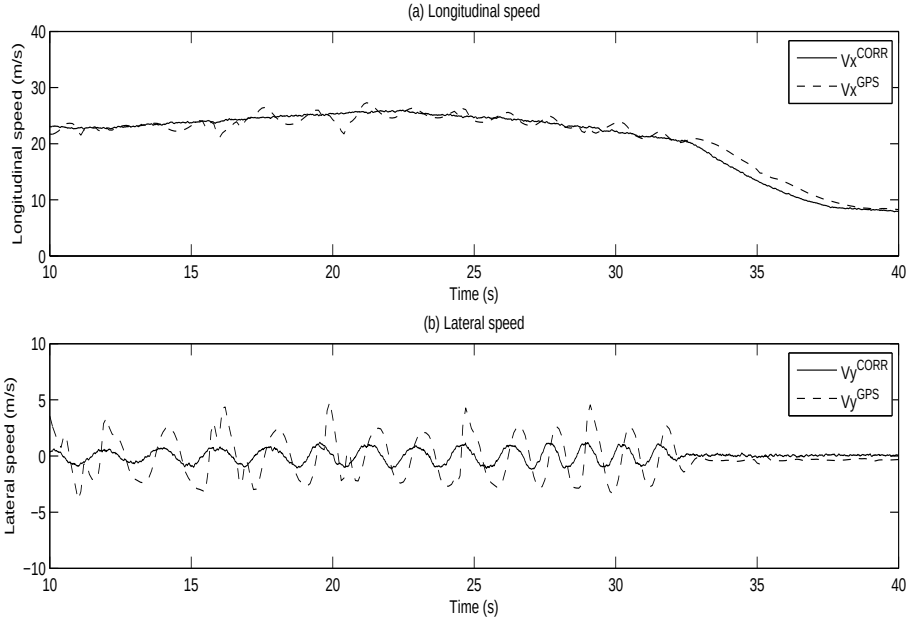

Figure 3.5: (a) Actual v_x and filtered v_x^{GPS} (b) Actual v_y and filtered v_y^{GPS}

Method 3: Applying a heuristic nonlinear filter to the time differentiated 10Hz position measurement.

The previous two methods lead to heavily phase-delayed velocity measurements, especially when the filters are configured to remove all noise components. For this reason, the idea of a task specific nonlinear filter is introduced. By looking at GPS data from several tests, it is possible to get an intuitive understanding of the structure of noise

seen in the velocity measurements. For example, Figure 3.2(b) shows that the noise usually comes in packets of two or three samples. This indicates that it should be possible to reduce noise significantly by evaluating a set of previous sample values and determining whether the current sample holds a realistic value or not. A few definitions:

U_k – filter input at current time k
Y_k – filter output at current time k
M_{Y_n} – mean value of n previous outputs
D_O – difference between current input and mean value of previous outputs

$$M_Y := M_{Y_3} = \frac{Y_{k-1} + Y_{k-2} + Y_{k-3}}{3} \tag{3.13}$$

$$D_O := |U_k - M_Y| \tag{3.14}$$

Equations 3.13-3.14 define parameters to be used in the filter. The main idea is that the filter should let measurements pass through without modifications when they are expected to be accurate. If an unrealistically large spike i detected in the input, however, the filter algorithm calculates an expected value of output instead. In practice, this means that the output is held constant when noise-bursts are detected.[1] In its simplest form, the algorithm becomes:

$$D_O \leq \kappa \Rightarrow Y_k = U_k \tag{3.15}$$

$$D_O > \kappa \Rightarrow Y_k = Y_{k-1} \tag{3.16}$$

κ is the number which determines how large the deviation between U_k and M_Y is allowed to be. If it is chosen very large, the filter will only be active for extreme noise conditions. An acceptable value has to be determined by logic and evaluation of empirical data. The filter should only modify the signal when it is noisy, which means that realistic vehicle accelerations must be tolerated. Longitudinal acceleration magnitude is largest for hard braking maneuvers. Consider a situation in which the vehicle brakes hard, and goes from 25 m/s to 0 m/s in three seconds. Assuming constant deceleration, the following relation holds:

$$\begin{aligned} a &= \frac{v_{x_2} - v_{x_1}}{t} \\ &= -8.33 m/s^2 \end{aligned}$$

[1] A predictive filter has also been developed, but because of minor stability problems, it won't be presented in this report.

When acceleration is constant and GPS measurements are perfect, the change between each sample is $a/10$ (10 Hz), and the braking maneuver gives:

$$\begin{aligned} D_I &= |U_k - M_Y| \\ &= \left| -\frac{2a}{\epsilon} \right| \\ &= 1.67 \end{aligned}$$

This example gives an indication of what value κ should be, at least for longitudinal velocity. Since acceleration measurements are available, κ can be made dynamic, defined as:

$$\kappa_x := \zeta_x \left| \frac{2a_x}{\epsilon} \right|, \ \zeta_x \geq 1 \tag{3.17}$$

$$\kappa_y := \zeta_y \left| \frac{2a_y}{\epsilon} \right|, \ \zeta_y \geq 1 \tag{3.18}$$

This ensures, at least theoretically, that the filter won't modify correct measurements. Note that practical experiments show that it is wise to chose ζ_x and ζ_y larger than 3. The reason for this, is that because three samples are evaluated, κ must reflect the sum of three consecutive acceleration measurements. Errors in the measurements are not considered. Naturally, a filter structure such as this doesn't remove all noise from the signal, but practical experiments show that it outperforms the linear filters by a large margin. Figure 3.6 and Figure 3.7 demonstrate the effectiveness of the heuristic approach. Notice that the filtered signals have no phase delay. This is because the output is calculated within the sample time interval defined by arrival of a new input. Numerical efficiency is equally good, since only a few simple expressions have to be solved for each sample. In the following sections, $\mathbf{v}^{GPS}$ will refer to the signal calculated by this filter, unless something else is explicitly stated.

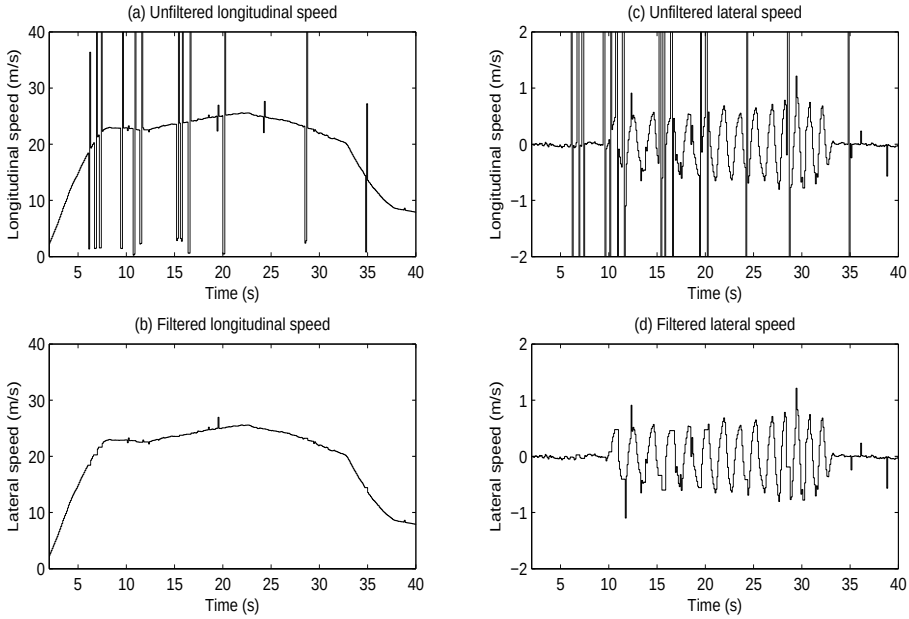

Figure 3.6: (a,c) Unfiltered v_x^{GPS} and v_y^{GPS} (b,d) Filtered v_x^{GPS} and v_y^{GPS}

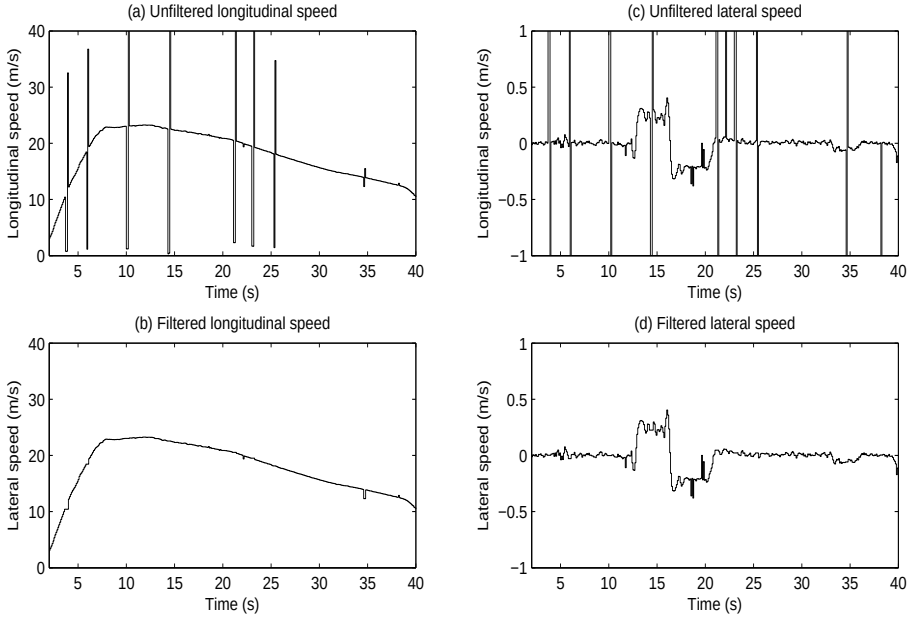

Figure 3.7: (a,c) Unfiltered v_x^{GPS} and v_y^{GPS} (b,d) Filtered v_x^{GPS} and v_y^{GPS}

3.2.2 Doppler based velocity determination

GPS-based velocity determination is usually done by aid of doppler carrier-phase processing. This approach eliminates the need for a differential implementation, by simply calculating the change of doppler phase (range) between two samples, and dividing this by sample time. It is possible to get doppler-based velocities for three dimensions, but as this is a receiver specific procedure, only absolute velocity will be considered here. A comparison between doppler velocity and actual absolute velocity [1] is shown in Figure 3.8. The test performed is a circle maneuver with high sideslip values, proving that the doppler method gives a very accurate representation of absolute velocity.

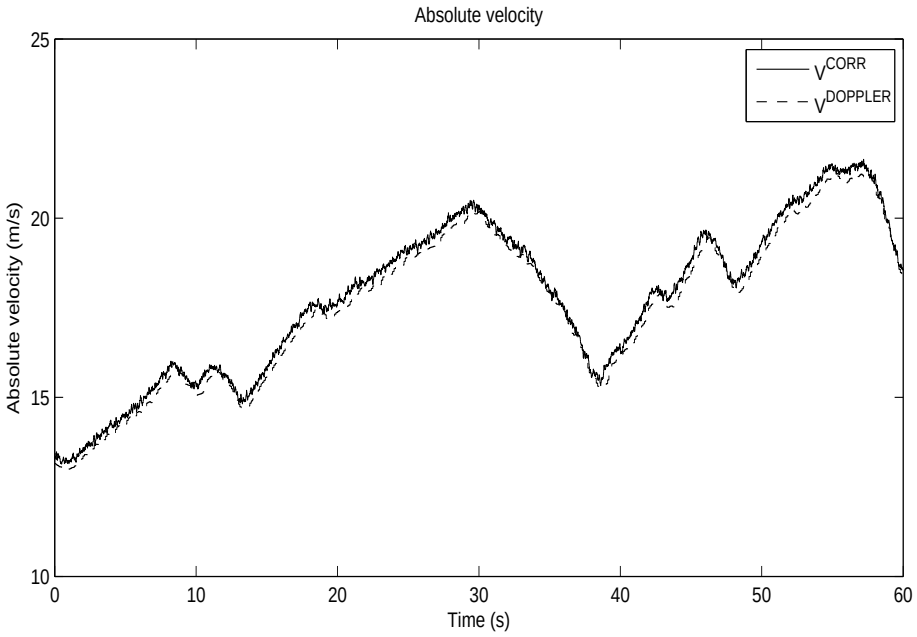

Figure 3.8: Comparison between GPS doppler velocity and actual absolute velocity

[1] Actual absolute velocity is computed as $V_A = \sqrt{v_x^2 + v_y^2}$, using the optical velocity measurements

Chapter 4

Observers

This chapter focuses on vehicle state estimation using nonlinear observers. Existing solutions, presented in [3], [4] and [25], are described, and new methods are developed - both GPS based and stand-alone approaches.

4.1 Non-adaptive observer

The non-adaptive observer presented in [3] takes the following form

$$\dot{\hat{v}}_x = a_x + r\hat{v}_y + \sum_{i=1}^{4} K_i(t)(v_{x,i} - \hat{v}_x) \tag{4.1}$$

$$\dot{\hat{v}}_y = a_y - r\hat{v}_x - K_{v_y}(ma_y - f_y(t, \hat{v}_x, \hat{v}_y, \hat{r})) \tag{4.2}$$

$$\dot{\hat{r}} = \frac{1}{J} f_r(t, \hat{v}_x, \hat{v}_y, \hat{r}) + K_r(r - \hat{r}) \tag{4.3}$$

As stated in [26], it is possible to write

$$\frac{\sum_{i=1}^{4} K_i(t) v_{x,i}}{K_{v_x}},\ K_{v_x}(t) := \sum_{i=1}^{4} K_i(t) \tag{4.4}$$

under the assumption that longitudinal velocity is measured perfectly. In this report, this will be referred to as **Assumption 4.1:** Error functions for f_y and f_r are defined

$$\tilde{f}_y(t, \tilde{v}_x, \tilde{v}_y, \tilde{r}) = f_y(t, v_x, v_y, r) - f_y(t, \hat{v}_x, \hat{v}_y, \hat{r})$$
$$\tilde{f}_r(t, \tilde{v}_x, \tilde{v}_y, \tilde{r}) = f_r(t, v_x, v_y, r) - f_r(t, \hat{v}_x, \hat{v}_y, \hat{r})$$

Now, the error dynamics can be written

$$\dot{\tilde{v}}_x = r\tilde{v}_y - K_{v_x}(t)\tilde{v}_x \tag{4.5}$$

$$\dot{\tilde{v}}_y = -r\tilde{v}_x + K_{v_y}\tilde{f}_y(t, \tilde{v}_x, \tilde{v}_y, \tilde{r}) \tag{4.6}$$

$$\dot{\tilde{r}} = \frac{1}{J}\tilde{f}_r(t, \tilde{v}_x, \tilde{v}_y, \tilde{r}) - K_r\tilde{r} \tag{4.7}$$

To prove stability, [3] uses the assumption that longitudinal velocity is measured perfectly, and that

$$\frac{\partial f_y}{\partial v_y}(t, v_x, v_y, r) \leq -c < 0 \tag{4.8}$$

The first assumption means that the estimate of v_x may become degraded when longitudinal wheel slips for all wheels are high. The second assumption means that convergence of $\tilde{v}_y$ depends on measured acceleration a_y. Since the non-adaptive observer is based on flat-earth dynamics, i.e. ϕ and θ equal zero, $\hat{v}_y$ will be biased when the vehicle experiences RBA. If the friction coefficient μ_H is wrong, all estimates will be degraded, and potentially useless if μ_H has large enough error. Figure 4.1 shows plots of v_y for a real life driving test, given by an optical measurement unit and the observer. Although the direct (optical) measurement is influenced by high-frequency noise, it gives an unbiased value of v_y, which can be used to test the correctness of the observer. It is easy to see that the two signals are different in the time period between 10 and 25 seconds. This is because the test vehicle experiences RBA in this interval. Here, the maximum friction coefficient μ_H has been set to 1, since the test was done on a high friction surface. Figure 4.2 shows what happens when μ_H is set to a lower (less correct) value. The observer with road-tire friction adaptation presented in [4] tries to deal with this problem by providing an estimate of μ_H

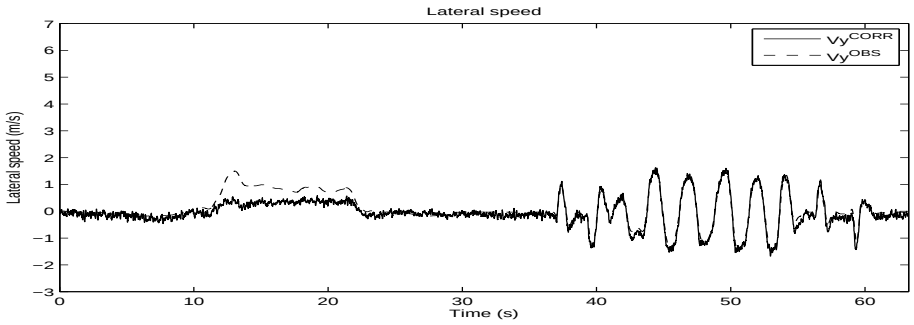

Figure 4.1: Test drive with RBA, $\mu_H = 1$

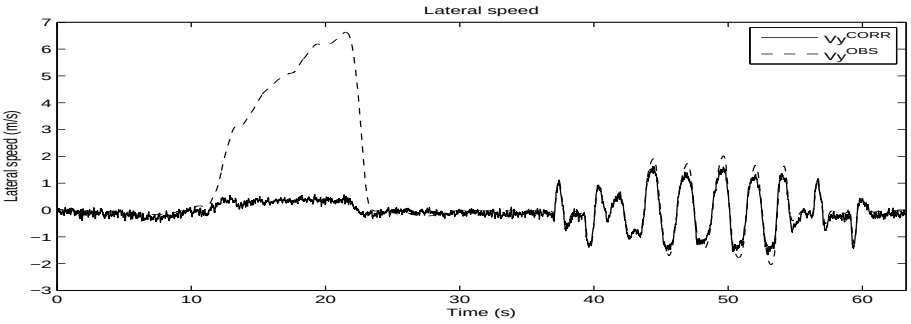

Figure 4.2: Test drive with RBA, $\mu_H = 0.8$

4.2 Adaptive observer

In [4], the estimate of lateral velocity uses feedback from a friction model based on friction adaptation. Since the state estimates have an identical structure to those presented in Section 4.1, the adaptive observer will only be described in a qualitative manner.

The main idea of road-tire friction adaptation is to provide a dynamic estimate of the generalized resultant force $f_y(t, v_x, v_y, r)$, which is used for feedback in equation 4.2. This force depends on the friction coefficient μ_H, represented by the parameter estimate $\hat{\theta}_\mu$, while v_x and r are assumed known, such that the expression becomes $f_y(t, v_y, \theta_\mu)$.

To prove stability, certain assumptions are made. It is stated that $f_y(t, v_y, \theta_\mu)$ can be written as a truncated Taylor series expansion, using $\hat{v}_y$ and $\hat{\theta_\mu}$ as arguments, and that this expansion is bounded and piecewise continuous in t, given that the estimation errors are small. It is also necessary that the vehicle is moving forward with high enough velocity, without rotating too fast. For a detailed discussion of all assumptions, see [4].

Without going into specifics about what can cause adaptation failure, it is easy to see, by looking at test results, that certain conditions can't be tolerated. Figure 4.3a shows that the estimate of v_y is sufficiently accurate when the car performs a circle maneuver on a flat, snowy surface. In 4.3b , however, a bias corresponding to RBA with $\phi = 2\,\mathrm{deg}$ is added to the acceleration measurement at 10 seconds. This is not a completely accurate representation of RBA, but illustrates how sensitive the adaptation scheme is to error in the acceleration measurement.

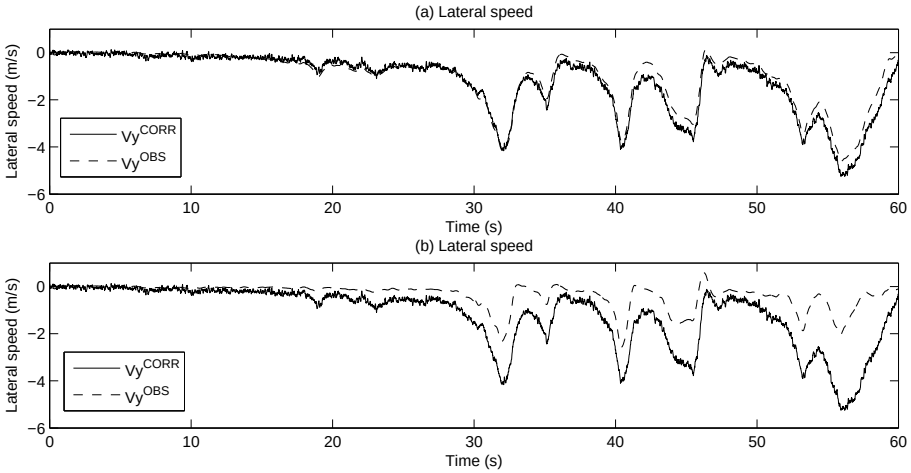

Figure 4.3: Circle maneuver, low friction. (a) Unbiased a_y. (b) Biased a_y

4.3 Augmented observer for road grade and bank angle estimation

To sum up the previous two sections: The non-adaptive observer is sensitive to errors in the user specified μ_H, especially if μ_H is chosen too low. If μ_H is higher than the actual surface conditions indicate, the estimate of v_y will be conservative, meaning that $\hat{v}_y$ is of lower magnitude than v_y when the vehicle is driven on a flat road.

The adaptive observer is very sensitive to errors in a_y, resulting in unpredictable behaviour of $\hat{v}_y$ and $\hat{\theta}_\mu$ when the vehicle experiences RBA. This is especially problematic in that the estimates depend on the sign of the acceleration bias, i.e. a right turn on a right banked road gives a too large value of $\hat{v}_y$, while a left turn on a left banked road gives a too small value of $\hat{v}_y$, even though the physical properties of these two maneuvers are identical. It is obvious that these effects have to be accounted for.

[25] lays the framework for an estimation structure which incorporates RBA in the observer equations, which are formulated as

$$\dot{\hat{v}}_y = a_y - r\hat{v}_x - \hat{w}_\phi - K_{v_y}(ma_y - f_y(t, v_x, \hat{v}_y, r)) \tag{4.9}$$

$$\dot{z} = -K_{v_y}(ma_y - f_y(t, v_x, \hat{v}_y, r)) \tag{4.10}$$

$$\hat{w}_\phi = K_w(\hat{v}_y - z - v_y^m) \tag{4.11}$$

Here, v_x and r are assumed known. Note that a new variable, v_y^m, has been included. In [25], this "measured" variable is actually a calculation of v_y, based on the friction model. The relations used are

$$a_y = \frac{1}{m} f_y(t, v_x, v_y, r)$$
$$v_y^m = f_y^{-1}(t, a_y, v_x, r)$$

Stability of this observer is proved using the assumption that v_y^m is a perfect measurement, so that it cancels out v_y terms in the error dynamics. Obviously, this can't be expected to hold in general, especially since v_y^m depends on the inverted friction model, which becomes nearly singular for high slips. This is where GPS enters the eqations. By using velocity measurements from a GPS receiver, v_y^m becomes completely independent of the observer equations. The following definition will be used

$$\mathbf{v}^m := \begin{bmatrix} v_x^m \\ v_y^m \\ v_z^m \end{bmatrix} \tag{4.12}$$
$$v_x^m := v_x^{GPS} \tag{4.13}$$
$$v_y^m := v_y^{GPS} \tag{4.14}$$
$$v_z^m := v_z^{GPS} \tag{4.15}$$

Now, a new approach to estimating v_x and v_y can be utilized. Let's first write out the new observer equations.

$$\dot{\hat{v}}_x = a_x + r\hat{v}_y - \hat{w}_\theta + K_{v_x}(t)(v_x - \hat{v}_x) \tag{4.16}$$
$$\dot{z_x} = K_{v_x}(t)(v_x - \hat{v}_x) \tag{4.17}$$
$$\hat{w}_\theta = K_{w_\theta}(\hat{v}_x - z_x - v_x^m) \tag{4.18}$$

$$\dot{\hat{v}}_y = a_y - r\hat{v}_x - \hat{w}_\phi - K_{v_y}(ma_y - f_y(t, \hat{v}_x, \hat{v}_y, r)) \tag{4.19}$$
$$\dot{z_y} = -K_{v_y}(ma_y - f_y(t, \hat{v}_x, \hat{v}_y, r)) \tag{4.20}$$
$$\hat{w}_\phi = K_{w_\phi}(\hat{v}_y - z_y - v_y^m) \tag{4.21}$$
$$\tag{4.22}$$

Note that $\dot{\hat{v}}_x$ and $\dot{\hat{v}}_y$ have been updated with information about RG and RBA respectively. Estimation errors are defined as

$$\tilde{v}_x := v_x - \hat{v}_x \tag{4.23}$$
$$\tilde{v}_y := v_y - \hat{v}_y \tag{4.24}$$
$$\tilde{w_\theta} := w_\theta - \hat{w_\theta} \ = w_\theta + K_{w_\theta}(z_x + \tilde{v}_x) \tag{4.25}$$
$$\tilde{w_\phi} := w_\phi - \hat{w_\phi} \ = w_\phi + K_{w_\phi}(z_y + \tilde{v}_y) \tag{4.26}$$

where the following assumptions have been made:

Assumption 4.2: v_x^m and v_y^m are perfect measurements.

$$v_x - v_x^m = 0$$
$$v_y - v_y^m = 0$$

Assumption 4.3: RG and RBA are constant.

$$\dot{\theta} = 0$$
$$\dot{\phi} = 0$$

The error dynamics are given by time differentiation of equations 4.23-4.26

$$\dot{\tilde{v}}_x = -\tilde{w_\theta} + r\tilde{v}_y - K_{v_x}(t)\tilde{v}_x \tag{4.27}$$
$$\dot{\tilde{v}}_y = -\tilde{w_\phi} - r\tilde{v}_x + K_{v_y}\tilde{f}_y(t, \tilde{v}_x, \tilde{v}_y, r) \tag{4.28}$$
$$\dot{\tilde{w}}_\theta = K_{w_\theta}(r\tilde{v}_y - \tilde{w_\theta}) \tag{4.29}$$
$$\dot{\tilde{w}}_\phi = -K_{w_\phi}(r\tilde{v}_x + \tilde{w_\phi}) \tag{4.30}$$

4.3.1 Stability analysis

Goals of the observer can be described in the following way:

Goal 1: Observer states, $\hat{\mathbf{x}}(t) = [\hat{v}_x \ \hat{v}_y \ \hat{w_\theta} \ \hat{w_\phi}]^T$, must all converge to the actual states $\mathbf{x}(t)$.

Goal 2: The origin of the observer error dynamics must be locally asymptotically stable.

To determine if these goals are achieved, traditional Lyapunov-theory will be used. First a Lyapunov function candidate (LFC) must be developed. This function has to meet certain demands to be classified as an actual Lyapunov function (LF). If analysis shows that these demands are met, the LFC is proven to be an actual LF, meaning that the origin of the observer error dynamics is asymptotically stable. Consider the following LFC:

$$V(\tilde{\mathbf{x}}) = \frac{1}{2}(\tilde{v}_x^2 + \tilde{v}_y^2 + \tilde{w}_\theta^2 + \tilde{w}_\phi^2) \tag{4.31}$$

If the conditions of *Theorem 4.10* in [27] hold for $V(\tilde{\mathbf{x}})$, it is an LF, and the origin of the observer error dynamics is exponentially stable. Note that $\frac{\partial V}{\partial t} = 0$, since V does not take t as an argument. Choosing $k_1 \leq \frac{1}{2}$, $k_2 \geq \frac{1}{2}$ and $a = 2$, the following inequalities hold

$$k_1 \left\|\tilde{\mathbf{x}}\right\|^a \;\leq\; V(\tilde{\mathbf{x}}) \;\leq\; k_2 \left\|\tilde{\mathbf{x}}\right\|^a \tag{4.32}$$

where $\|\tilde{\mathbf{x}}\|$ is the Euclidian norm of $\tilde{\mathbf{x}}$. This proves that the first condition of exponential stability holds. To evaluate the second condition, $\dot{V}$ is calculated:

$$\begin{aligned}
\dot{V} = &\tilde{v}_x(-\tilde{w}_\theta + r\tilde{v}_y - K_{v_x}(t)\tilde{v}_x) \\
&+ \tilde{v}_y(-\tilde{w}_\phi - r\tilde{v}_x + K_{v_y}\tilde{f}_y(t, \tilde{v}_x, \tilde{v}_y, r)) \\
&+ \tilde{w}_\theta(K_{w_\theta}(r\tilde{v}_y - \tilde{w}_\theta)) \\
&+ \tilde{w}_\phi(-K_{w_\phi}(r\tilde{v}_x + \tilde{w}_\phi)) \\
\\
= &- K_{v_x}(t)\tilde{v}_x^2 - K_{w_\theta}\tilde{w}_\theta^2 - K_{w_\phi}\tilde{w}_\phi^2 - \tilde{v}_x\tilde{w}_\theta - \tilde{v}_y\tilde{w}_\phi \\
&+ K_{w_\theta}r\tilde{v}_y\tilde{w}_\theta - K_{w_\phi}r\tilde{v}_x\tilde{w}_\phi + K_{v_y}\tilde{f}_y(t, \tilde{v}_x, \tilde{v}_y, r)\tilde{v}_y
\end{aligned}$$

The last term depends on $\tilde{f}_y$, and should be rewritten. According to *Lemma 1* in [3], it is possible to state the following assumption:

Assumption 4.4: The friction model is continuously differentiable with regards to $\tilde{v}_y$ and $\tilde{v}_x$, and bounded by positive constants c_1 and c_2, such that:

$$\tilde{v}_y\tilde{f}_y(t, \tilde{v}_x, \tilde{v}_y, r) \leq -c_1\tilde{v}_y^2 + c_3|\tilde{v}_x||\tilde{v}_y|$$

Substituting this into $\dot{V}$, gives

$$\begin{aligned}\dot{V} \leq & -K_{v_x}(t)\tilde{v}_x^2 - \tilde{v}_x\tilde{w}_\theta - K_{w_\theta}\tilde{w}_\theta^2 - c_1K_{v_y}\tilde{v}_y^2 + c_3K_{v_y}|\tilde{v}_x||\tilde{v}_y| \\ & - \tilde{v}_y\tilde{w}_\phi - K_{w_\phi}\tilde{w}_\phi^2 + K_{w_\theta}r\tilde{v}_y\tilde{w}_\theta - K_{w_\phi}r\tilde{v}_x\tilde{w}_\phi\end{aligned}$$

This inequality can be upper bounded by expressing the right hand side in terms of $|\tilde{\mathbf{x}}|$, assuming $|r| < r_u$, $K_x = \mathbf{min}(K_{v_x}(t))$, $K_y = K_{v_y}$, where r_u denotes a physical upper bound on yaw-rate, in the following way:

$$\begin{aligned}\dot{V} \leq & -K_x\tilde{v}_x^2 + |\tilde{v}_x||\tilde{w}_\theta| - K_{w_\theta}\tilde{w}_\theta^2 - c_1K_y\tilde{v}_y^2 + c_3K_y|\tilde{v}_x||\tilde{v}_y| \\ & + |\tilde{v}_y||\tilde{w}_\phi| - K_{w_\phi}\tilde{w}_\phi^2 + K_{w_\theta}r_u|\tilde{v}_y||\tilde{w}_\theta| + K_{w_\phi}r_u|\tilde{v}_x||\tilde{w}_\phi| \\ = & -|\tilde{\mathbf{x}}|^T\mathbf{A}|\tilde{\mathbf{x}}|\end{aligned}$$

If the matrix $\mathbf{A}$ is positive definite, and k_3 is a positive constant such that

$$k_3 \leq \lambda_{\mathbf{A}}^{min}$$

where $\lambda_{\mathbf{A}}^{\min}$ denotes the smallest eigenvalue of $\mathbf{A}$, $\dot{V}$ satisfies the second condition of exponential stability, which in this case becomes:

$$\dot{V}(\tilde{\mathbf{x}}) \ \leq -|\tilde{\mathbf{x}}|^T\mathbf{A}|\tilde{\mathbf{x}}| \ \leq -k_3\left\|\tilde{\mathbf{x}}\right\|^a \tag{4.33}$$

The matrix $\mathbf{A}$ is defined as:

$$\mathbf{A} := \begin{bmatrix} K_x & -\frac{1}{2}c_3K_y & -\frac{1}{2} & -\frac{1}{2}K_{w_\phi}r_u \\ -\frac{1}{2}c_3K_y & c_1K_y & -\frac{1}{2}K_{w_\theta}r_u & -\frac{1}{2} \\ -\frac{1}{2} & -\frac{1}{2}K_{w_\theta}r_u & K_{w_\theta} & 0 \\ -\frac{1}{2}K_{w_\phi}r_u & -\frac{1}{2} & 0 & K_{w_\phi} \end{bmatrix} \tag{4.34}$$

The proof is concluded if $\mathbf{A}$ can be shown to be positive definite. *Theorem 3.7* in [28] states that a symmetric $n \times n$ matrix $\mathbf{A}$ is positive definite if all the leading principal minors are positive. Calculating the principal minors, denoted $d_i, i = 1, ..., 4$, gives:

$$d_1 = K_x \tag{4.35}$$

$$d_2 = K_x c_1 K_y - \frac{1}{4} c_3 K_y^2 \tag{4.36}$$

$$d_3 = K_x c_1 K_y K_{w_\theta} - \frac{1}{4} K_x K_{w_\theta}^2 r_u^2 - \frac{1}{4} c_3 K_y K_{w_\theta} r_u - \frac{1}{4} c_3^2 K_y^2 K_{w_\theta} - \frac{1}{4} c_1 K_y \tag{4.37}$$

$$\begin{aligned} d_4 = {} & K_x c_1 K_y K_{w_\theta} K_{w_\phi} - \frac{1}{4} K_x K_{w_\theta}^2 r_u^2 K_{w_\phi} - \frac{1}{4} K_x K_{w_\theta} \\ & - \frac{1}{4} c_3^2 K_y^2 K_{w_\theta} K_{w_\phi} - \frac{1}{2} c_3 K_y K_{w_\theta} r_u K_{w_\phi} + \frac{1}{16} - \frac{1}{4} c_1 K_y K_{w_\phi} \\ & - \frac{1}{8} K_{w_\theta} r_u K_{w_\phi} - \frac{1}{4} K_{w_\phi}^2 r_u^2 c_1 K_y K_{w_\theta} + \frac{1}{16} K_{w_\phi}^2 r_u^4 K_{w_\theta}^2 \end{aligned} \tag{4.38}$$

The goal is to find the set of gains which yields $d_i > 0, i = 1, ..., 4$. At this juncture, it is constructive to realize the potential of finding one configuration which makes **A** positive definite. By doing this, the existence of *at least one* set of stabilizing gains is proven. While not a mathematically satisfying solution, it is of practical value, considering that gain-tuning for physical systems is largely an empirical science. Another motivating factor, is that the stability analysis is largely based on assumptions about properties of the physical system; when these assumptions no longer hold, stability proofs fail, which in turn means that the correctness of a proof is non-deterministic. With this in mind, an approach to finding one set of stabilizing gains is presented.

By stating $K_y > 0$, it can immediately be seen from d_1 and d_2 that

$$K_x > \frac{1}{4c_1} K_y c_3^2 \tag{4.39}$$

These are the criteria used for gain selection in [3]. Intuitively, the observer presented in this section should have roughly the same performance as the non-adaptive observer when the vehicle does not experience RG and RBA. This indicates that the gains K_{w_θ} and K_{v_ϕ} can be chosen for a configuration in which the non-adaptive observer is not degraded. If it is degraded, K_{w_θ} and K_{v_ϕ} can't be used to improve stability either way. The constants c_1, c_3 and r_u govern stability properties. By reviewing test results in which the non-adaptive observer fails, practical values of c_1, c_3 and r_u can be estimated. Figure 4.4 shows results of a flat surface test with high-dynamics and low friction, using the non-adaptive observer. Observer failure is easily identified, and by inspecting internal states, it can be seen that the follwing bounds give an approximation to conditions which must be tolerated:

$$c_1 > 1$$
$$c_3 < 1$$
$$r_u < 1\, rad/s$$

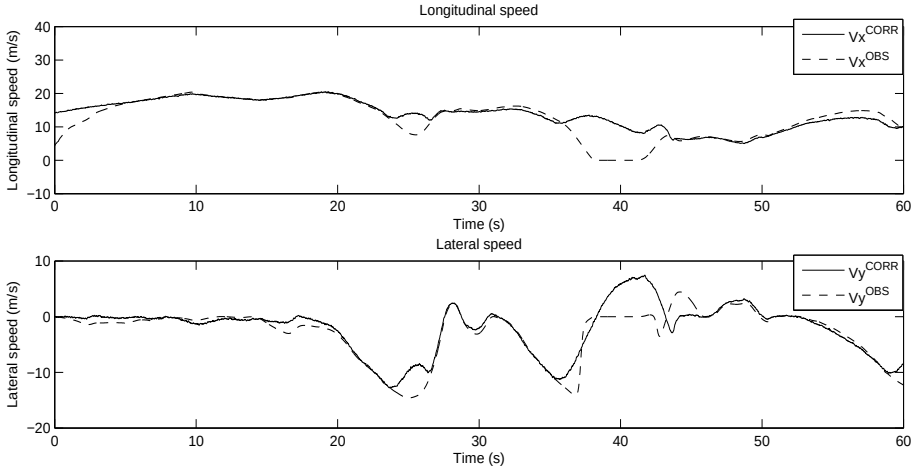

Figure 4.4: Circle maneuver on ice

After some experimentation, it is discovered that the gains can be chosen as:

$$K_y = 1$$
$$K_x = 3$$
$$K_{w_\theta} = 1$$
$$K_{w_\phi} = 1$$

To verify correctness, the gains can be substituted into equations 4.35-4.38, along with the bounds on c_1, c_3 and r_u. Since $d_i > 0, i = 1, ..., 4$, the origin of the observer error dynamics is proven to be locally exponentially stable for at least one set of feedback gains. This analysis does not allow stating that **Goal 1** and **Goal 2** have been achieved, but it has been shown that the observer can be made stable as long as certain physical properties hold. While the theoretical implications are small, an implementation of the observer for test purposes is justified.

4.4 Roll observer

A GPS based approach to RBA compensation is realistic, but still a bit luxurious. With this in mind, an observer scheme based on vehicle roll dynamics is developed. The idea is that a roll rate gyro can give some information about the road structure. In any case, a good estimate of vehicle roll can be used to correct gravity based errors in the lateral acceleration measurement. To implement a vehicle roll observer, it is convenient to express the dynamics on standard state-space form, using a temporary variable change.

$$\mathbf{x}_\phi := \begin{bmatrix} v_y & x_1 & x_2 \end{bmatrix}^T = \begin{bmatrix} v_y & \phi_v & \dot{\phi}_v \end{bmatrix}^T \tag{4.40}$$

$$f_y = f_y(t, v_x, v_y, r) \tag{4.41}$$

$$\hat{f}_y = \hat{f}_y(t, v_x, \hat{v}_y, r) \tag{4.42}$$

$$\tilde{f}_y = \tilde{f}_y(t, v_x, \tilde{v}_y, r) \tag{4.43}$$

Now, equation 2.25 can be written as

$$\dot{x}_1 = x_2 \tag{4.44}$$

$$\dot{x}_2 = \frac{1}{J_x}[f_y h + (mgh - C_\phi + r^2(J_y - J_z))x_1 - K_\phi x_2] \tag{4.45}$$

This model is based on familiar mass-spring-damper dynamics. Development of an observer is simplified by making two realistic assumptions.

Assumption 4.5: v_x and r are known, and some form of roll rate measurement is available

Assumption 4.6: Roll angles are small enough for $\sin\phi \approx \phi$ to hold

The following observer is proposed

$$\dot{\hat{v}}_y = a_y - r v_x - g\hat{x}_1 - K_{v_y}(ma_y - \hat{f}_y) \tag{4.46}$$

$$\dot{\hat{x}}_1 = \hat{x}_2 \tag{4.47}$$

$$\dot{\hat{x}}_2 = \frac{1}{J_x}[\hat{f}_y h + (mgh - C_\phi + r^2(J_y - J_z))\hat{x}_1 - K_\phi \hat{x}_2] + K_2[x_2 - \hat{x}_2] \tag{4.48}$$

The error dynamics are

$$\dot{\tilde{v}}_y = -g\tilde{x}_1 + K_{v_y}\tilde{f}_y \tag{4.49}$$
$$\dot{\tilde{x}}_1 = \tilde{x}_2 \tag{4.50}$$
$$\dot{\tilde{x}}_2 = \frac{1}{J_x}[\tilde{f}_y h + (mgh - C_\phi + r^2(J_y - J_z))\tilde{x}_1 - (K_\phi + K_2 J_x)\tilde{x}_2] \tag{4.51}$$

To get an idea about stability properties of the observer, an LFC will be evaluated.

$$V = \frac{1}{2}({v_y}^2 + {\tilde{x}_1}^2 + {\tilde{x}_2}^2 + a\tilde{x}_1\tilde{x}_2) \tag{4.52}$$

where a is a positive constant such that

$${\tilde{x}_1}^2 + {\tilde{x}_2}^2 + a\tilde{x}_1\tilde{x}_2 > 0, \forall \tilde{x}_1, \tilde{x}_2 \neq 0$$

This is true for

$$0 < a < 2$$

The expression of the time derivative of V determines stability.

$$\begin{aligned}\dot{V} = &- g\tilde{v}_y\tilde{x}_1 + K_{v_y}\tilde{v}_y\tilde{f}_y + \frac{h}{J_x}\tilde{x}_2\tilde{f}_y + \frac{ah}{J_x}\tilde{x}_1\tilde{f}_y + \frac{a}{J_x}(mgh - C_\phi + r^2(J_y - J_z))\tilde{x}_1{}^2 \\ &+ \frac{1}{J_x}(mgh - C_\phi + r^2(J_y - J_z) + J_x - aK_\phi - aJ_xK_2)\tilde{x}_1\tilde{x}_2 - (\frac{K_\phi}{J_x} + K_2 - a){\tilde{x}_2}^2\end{aligned}$$

Assumption 4.4 must be used to rewrite the cross terms $\tilde{v}_y\tilde{f}_y$, $\tilde{x}_1\tilde{f}_y$ and $\tilde{x}_2\tilde{f}_y$. Note that $\tilde{v}_x$ is zero for this observer, and that $|\tilde{f}_y| \leq c_1|\tilde{v}_y|$ is implied by the assumption. For simplicity, the following variable change is used

$$\alpha_1 = -(mgh - C_\phi + r^2(J_y - J_z))$$

which results in

$$\begin{aligned}\dot{V} \leq &- g\tilde{v}_y\tilde{x}_1 - c_1K_{v_y}{\tilde{v}_y}^2 + \frac{ahc_1}{J_x}\tilde{x}_1|\tilde{v}_y| + \frac{hc_1}{J_x}\tilde{x}_2|\tilde{v}_y| - \frac{a\alpha_1}{J_x}{\tilde{x}_1}^2 \\ &- \frac{1}{J_x}(\alpha_1 + a(K_\phi + J_xK_2) - J_x)\tilde{x}_1\tilde{x}_2 - (\frac{K_\phi}{J_x} + K_2 - a){\tilde{x}_2}^2\end{aligned}$$

It is necessary to make another technical assumption.

Assumption 4.7: $\alpha_1 > 0$ and $-\frac{1}{J_x}(\alpha_1 + a(K_\phi + J_x K_2) - J_x) \leq -s_1 < 0$

This assumption will be correct for all practical values of C_ϕ. Writing $\dot{V}$ in matrix form is convenient for analysis, but the current expression requires that absolute values of the error states are used. This creates an upper bound for $\dot{V}$.

$$\begin{aligned}\dot{V} \leq & - c_1 K_{v_y} {\tilde{v}_y}^2 - \frac{a\alpha_1}{J_x}{\tilde{x}_1}^2 - (\frac{K_\phi}{J_x} + K_2 - a){\tilde{x}_2}^2 \\ & + \frac{1}{J_x}(ahc_1 + gJ_x)|\tilde{v}_y||\tilde{x}_1| + \frac{hc_1}{J_x}|\tilde{v}_y||\tilde{x}_2| + s_1|\tilde{x}_1||\tilde{x}_2|\end{aligned} \tag{4.53}$$

In matrix form:

$$\dot{V} = -|\mathbf{x}_\phi|^T \mathbf{P} |\mathbf{x}_\phi|$$

where $\mathbf{P}$ is a symmetric 3×3 matrix. If $\mathbf{P}$ is positive definite, the observer is globally exponentially stable. Criteria for positive definiteness were stated in the previous section.

$$\mathbf{P} = \begin{bmatrix} c_1 K_{v_y} & -\frac{1}{2J_x}(ahc_1 + gJ_x) & -\frac{hc_1}{2Jx} \\ -\frac{1}{2J_x}(ahc_1 + gJ_x) & \frac{a\alpha_1}{J_x} & -\frac{1}{2}s_1 \\ -\frac{hc_1}{2Jx} & -\frac{1}{2}s_1 & (\frac{K_\phi}{J_x} + K_2 - a) \end{bmatrix}$$

The leading principal minors of $\mathbf{P}$ are

$$d_1 = c_1 K_{v_y} \tag{4.54}$$

$$d_2 = \frac{1}{J_x}(a\alpha_1 c_1 K_{v_y} - \frac{1}{4J_x}(ahc_1 + gJ_x)^2) \tag{4.55}$$

$$\begin{aligned} d_3 = & c_1 K_{v_y}\left[\frac{a\alpha_1}{J_x}\left(\frac{K_\phi}{J_x} + K_2 - a\right) - \frac{1}{4}{s_1}^2\right] \\ & - \frac{1}{2J_x}(ahc_1 + gJ_x)\left[\frac{1}{2J_x}(ahc_1 + gJ_x)\left(\frac{K_\phi}{J_x} + K_2 - a\right) + \frac{hc_1 s_1}{4J_x}\right] \\ & - \frac{hc_1}{2J_x}\left[\frac{s_1}{4J_x}(ahc_1 + gJ_x) + \frac{a\alpha_1 hc_1}{2{J_x}^2}\right] \end{aligned} \tag{4.56}$$

Since d_1, d_2 and d_3 have to be positive for P to be positive definite, K_{v_y} and K_2 must be specified to meet this demand. The first two minors give

$$K_{v_y} > \frac{(ahc_1 + gJ_x)^2}{4a\alpha_1 c_1 J_x} > 0 \tag{4.57}$$

The expression for d_3 is quite complicated, so determining absolute bounds on the gains is impractical *for this LFC*, especially considering how conservative inequality 4.53 is. However, it is apparent that the first term of d_3 can be made positive by selecting K_2 correctly, which in turn means that selecting K_{v_y} large enough will make d_3 positive. The follwing inequality states the necessary bound on K_2 with regards to the analysis performed in this section

$$K_2 > \frac{J_x {s_1}^2}{a\alpha_1} - \frac{K_\phi}{J_x} + a \tag{4.58}$$

Without further analysis, it is stated that the roll observer can be made asymptotically stable by gain selection. Usefulness can be determined through simulations.

4.4.1 Bank angle estimation

At this point, it is appropriate to make an attempt at tackling the real issue at hand - acceleration measurement errors due to road bank angle. The term bank angle is somewhat misleading, as it is the vehicle's orientation on the surface of the road which is important, not the road angle itself. For the problem to be reasonably managable, an assumption has to be made.

Assumption 4.8: Whenever the road bank angle changes, the vehicle is parallel to the road (no sideslip), meaning that the change is visible in a roll rate gyro.

The motivation for this assumption stems from vehicle kinematics. To illustrate: If the vehicle changes orientation, for example due to large sideslip on a low friction surface, when the bank angle is constant with magnitude larger than zero, the gravitational bias experienced by accelerometer a_y may become significantly smaller than the road bank angle indicates. However, the bank angle estimate won't be affected, as this maneuver only gives a visible change in dynamic roll ϕ_v. When the vehicle recovers from this undesired event and returns to driving straight ahead, the bank angle estimate will be correct.

The mathematics of the roll observer in the previous section is only concerned with rolling motion of the vehicle chassis relative to the wheels, not bank angle. A roll gyro measurement will under Assumption 4.8 include change in bank angle. This leads to the following relation:

$$\dot{\phi}_r \approx p_d - \dot{\phi}_v \tag{4.59}$$

Using $p_d = x_2$, with x_2 as defined in the previous section, an observer with bank angle compensation is specified.

$$\dot{\hat{v}}_y = a_y - rv_x - g(\hat{x}_1 + \hat{\phi}_r) - K_{v_y}(ma_y - \hat{f}_y) \tag{4.60}$$

$$\dot{\hat{x}}_1 = \hat{x}_2 \tag{4.61}$$

$$\dot{\hat{x}}_2 = \frac{1}{J_x}[\hat{f}_y h + (mgh - C_\phi + r^2(J_y - J_z))\hat{x}_1 - K_\phi \hat{x}_2] + K_2[x_2 - \hat{x}_2] \tag{4.62}$$

$$\dot{\hat{\phi}}_r = K_3[x_2 - \hat{x}_2] \tag{4.63}$$

Showing stability of this observer has proved difficult, so instead of including an incomplete mathematical analysis, the observer will be evaluated by aid of simulations.

Chapter 5

Experimental results and discussion

When combining the various results presented in this report, there are four main criteria which determine practical usefulness.

Criterion 1: GPS-based velocity measurements must give a *reasonably* accurate approximation to actual vehicle velocity.

Criterion 2: The augmented observer must work perfectly when μ_H is specified correctly and $v^m = v^{CORR}$.

Criterion 3: The augmented observer must have *acceptable* performance when μ_H is specified correctly and $v^m = v^{GPS}$.

Criterion 4: Implementation of the bank angle observer must improve estimates of v_y for all conditions. Tests are performed using the CASCaDE simulator.

The following sections demonstrate how these criteria compare to test results, both positively and negatively. Naturally, the wide array of configurable parameters affecting performance of each test won't be printed out, as this would distract from understanding of general results. However, it is necessary to state properties of three key parameters:

K_{w_θ} – Set to one
K_{w_ϕ} – Set to one
μ_H – Chosen to match known surface conditions

If different configurations are used, they wille be specified explicitly.

5.1 Criterion 1

The first criterion can be expected to hold when vehicle sideslip is low. This is because $\psi_c \approx \psi$. Test conditions should therefore be $\mu_H \approx 1$, $\theta = 0$ and $\phi = 0$. Figure 5.1 shows results of a test where these conditions hold.

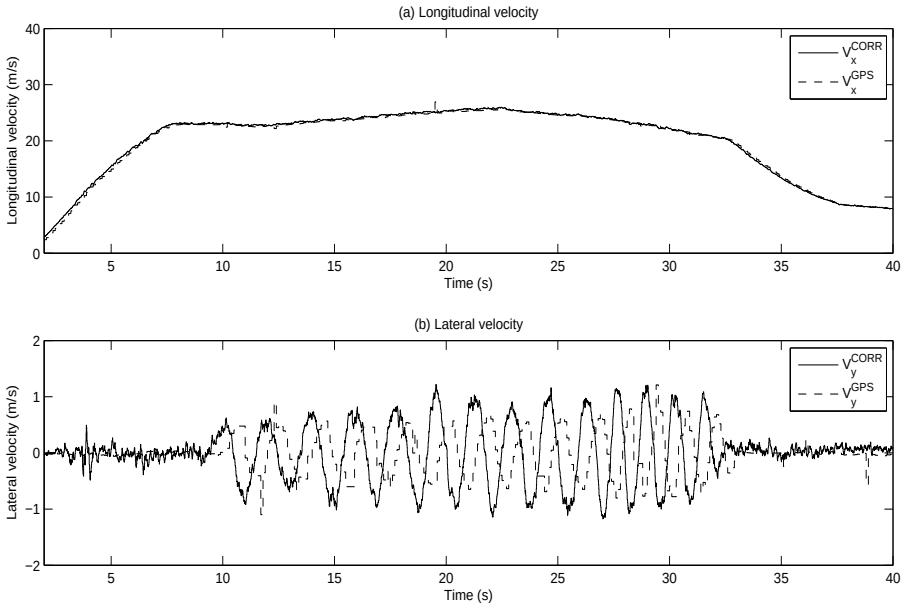

Figure 5.1: (a) Actual v_x and filtered v_x^{GPS} (b) Actual v_y and filtered v_y^{GPS}

The vehicle performs a slalom maneuver. While the shape of v_y^{GPS} gives a good approximation to actual v_y, it is unfortunately corrupted by time delay (0.5 s). Recalling from Section 3.2 that the heuristic filter does not give any extra phase to the signal, the conclusion is that the time delay stems from intrinsic properties of the GPS system. Using the current configuration, this delay can't be accounted for by software manipulation, rendering v_y^{GPS} a poor candidate for feedback in the observer.

Although the negative implications of this result are overshadowing, it is wise to analyze how v_y^{GPS} performs with respect to other properties, since it is possible that the time delay can be decreased significantly, e.g. by using a higher update frequency in the receiver.

The amplitude of v_y^{GPS} is slightly lower than that of actual v_y. Here, the main culprit is expected to be error in ψ_c, considering that the vehicle most likely experiences some degree of sideslip for lateral velocities of this magnitude. The definition of sideslip, is as follows:

$$\beta := \psi - \psi_c \tag{5.1}$$

Since the current observer implementation produces an estimate of sideslip, it is possible to use ψ instead of ψ_c in $\mathbf{R}_b^n$, by setting $\psi = \psi_c + \beta$. A practical implementation of this, requires that β is delayed correspondingly to the time-delay of the GPS measurements. Figures 5.2 and 5.3 show what happens when this approach is utilized. Note that v_y has been delayed to make signal comparison easier.

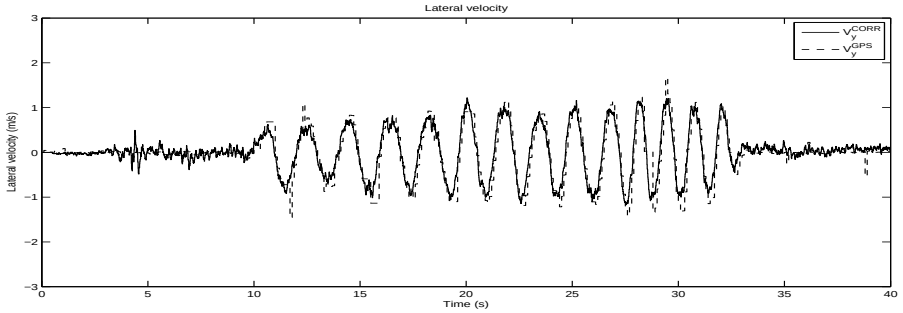

Figure 5.2: Actual v_y and filtered v_y^{GPS}, using feedback from sideslip

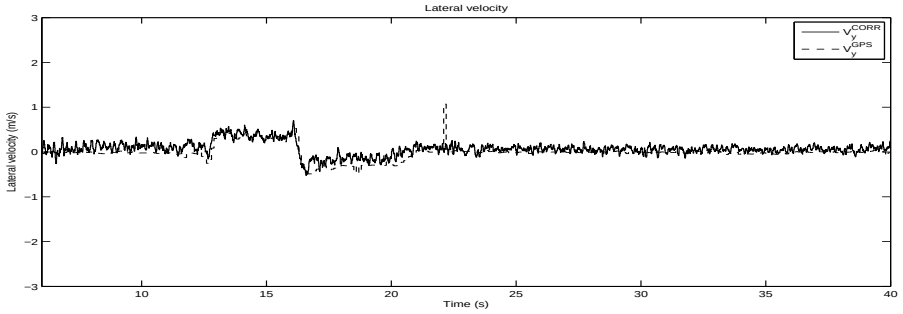

Figure 5.3: Actual v_y and filtered v_y^{GPS}, using feedback from sideslip

In short, Criterion 1 will hold if GPS time delays can be reduced to an acceptable level. For the data sets used in this report, however, Criterion 1 fails.

5.2 Criterion 2

The second criterion states that when a correct measurement of v_y is used, the augmented observer should be able to handle variations in RBA and RG, given a correct specification of μ_H.

Figure 4.1 demonstrated how the non-adaptive observer was affected by RBA. If the augmented observer is to be of use, it has to remove the RBA-error component from $\hat{v}_y$. Figure 5.4 shows the same maneuver, using the augmented observer with feedback from v_y^{CORR}. Observer error is well within accepted margins, showing that for this particular test, the augmented observer has desired performance. Unfortunately, actual RBA values are unknown, so the correctness of $\hat{w}_\phi$ can't be confirmed without new test data sets.

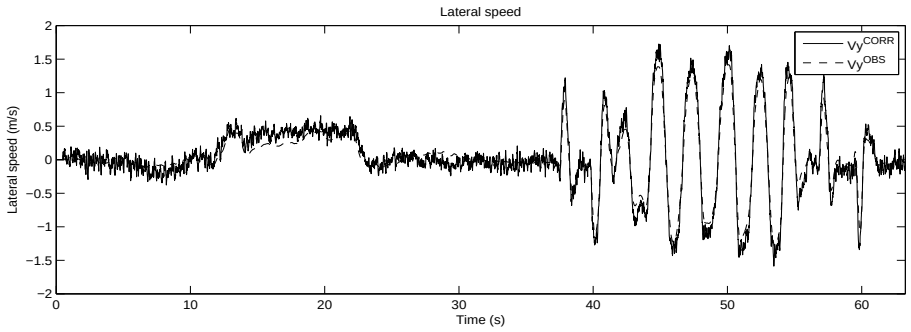

Figure 5.4: Actual v_y and $\hat{v}_y$

To verify, another data set is evaluated. In Figure 5.5, it can be seen that the non-adaptive observer gives a very large error in $\hat{v}_y$ towards the end. This error is caused by RBA. By comparison, the augmented observer works close to perfectly, as seen in Figure 5.6.

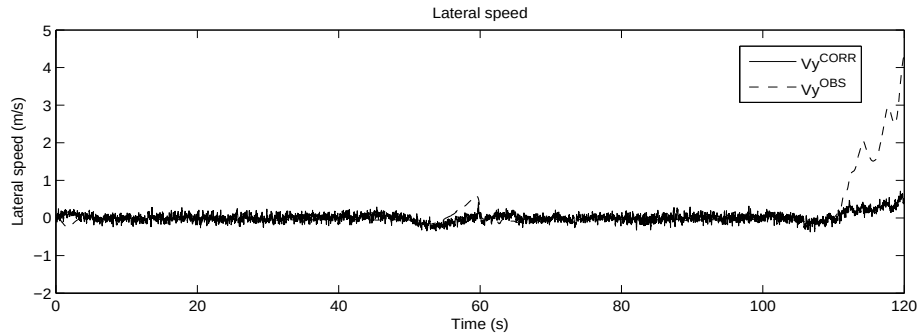

Figure 5.5: Actual v_y and $\hat{v}_y$, non-adaptive observer

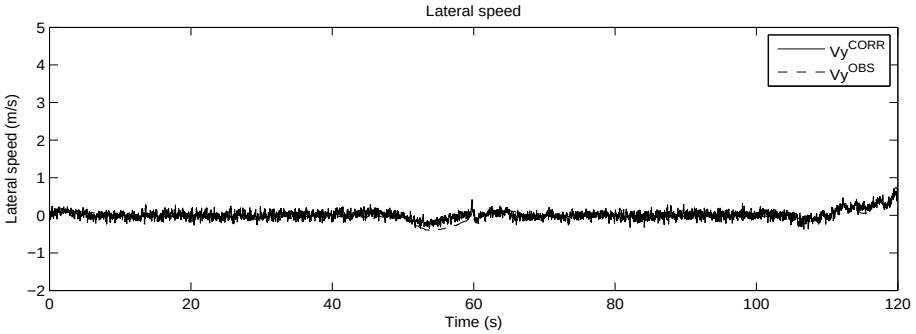

Figure 5.6: Actual v_y and $\hat{v}_y$, augmented observer

Because none of the data sets currently available contain tests performed with RG, correctness of $\hat{v}_x$ and $\hat{w}_\theta$ can't be shown directly. However, by adding a slowly varying sinus signal to a_x, the estimation error caused by RG can be simulated. To boldly go where few vehicles will, the sinus signal is given an amplitude corresponding to $\theta = 20$ degrees, which is an extreme and unlikely road condition. Figure 5.7 shows what happens to the non-adaptive estimate of longitudinal velocity in this case.

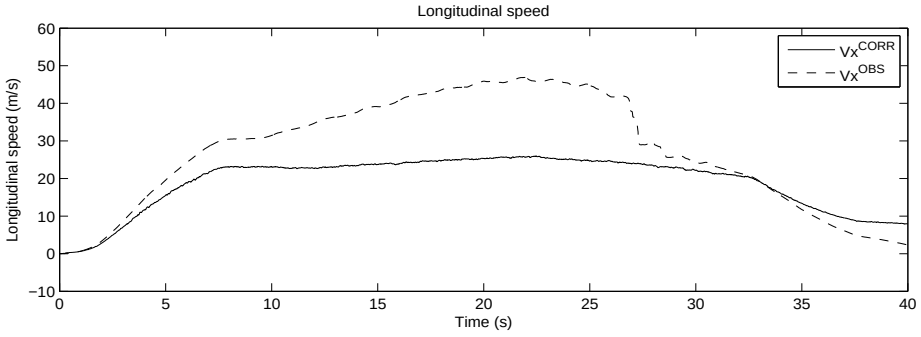

Figure 5.7: Actual v_x and $\hat{v}_x$, non-adaptive observer

Performing the same test with the augmented observer, gives an expected result. $\hat{v}_x$ converges to the correct value, and $\hat{w}_\theta$ gives a very good indication of what the actual RG is, although variations in lateral velocity and sideslip induce some oscillations. See Figure 5.8.

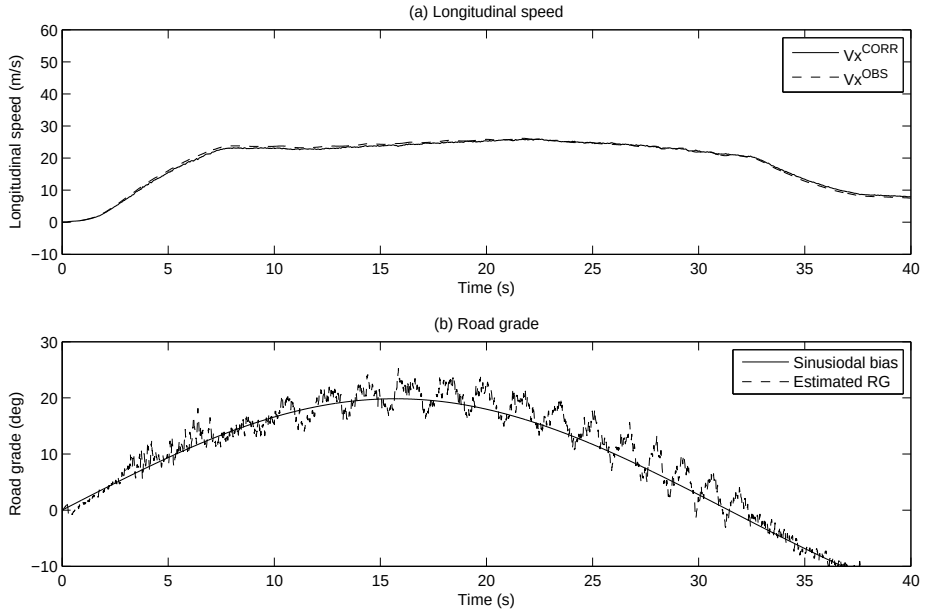

Figure 5.8: (a) Actual v_x and $\hat{v}_x$, augmented observer (b) Acceleration bias and estimated RG

In this section, it has been shown that Criterion 2 holds. This is only important in that it demonstrates correctness of the augmented observer when v^m is correct, which is a fundamental requirement of the estimation scheme.

5.3 Criterion 3

The conditional failure of Criterion 1 indicates that Criterion 3 should suffer the same fate. Luckily, things are not quite that black and white. Failure of Criterion 1 was based on the GPS based velocity signal's lack of ability to track high dynamic maneuvers correctly, due to an inherent time delay in the system. While the augmented observer is expected to have reduced performance when the vehicle experiences fast changes in acceleration, it should still be able to compensate for RG and RBA when these disturbances vary slowly. Still, a few proverbial bumps in the road have to be considered:

- The rotation matrix $\mathbf{R}_b^n$ currently in use, does not include information about ϕ and θ. In practice, this means that v_x^{GPS} and v_y^{GPS} actually give receiver velocity components in a horizontal plane. If e.g. the vehicle is driven up a steep hill, v_x^{GPS} will become significantly lower than actual v_x. The most immediate solution to this problem, is simply to use feedback of estimated ϕ and θ, from the augmented observer, in $\mathbf{R}_b^n$.

- While v_x^{GPS} will be a good approximation to v_x most of the time, v_y^{GPS} can corrupt $\hat{v}_y$ significantly due to time delay. Disregarding the limiting choice of gains used in the stability proof in Section 4.3, K_{w_ϕ} should be set fairly low, that is $K_{w_\phi} < 1$. Knowing that this gain determines to what degree the GPS measurement is allowed to influence the state estimation, justifies experiments with lower values. All tests in this section are based on $K_{w_\phi} = \frac{1}{2}$.

- For certain tests, the GPS measurement is extremely corrupted. If an actual implementation of the results from this report is to be considered, some form of software procedure which discovers GPS failure has to be developed.

To begin with something familiar, the test shown in Figure 4.1 is presented once again, this time using the augmented observer with feedback from GPS based velocities. Desired behaviour is correction of error due to RBA, and acceptable magnitude of degradation due to GPS time delay. See Figure 5.9 and Figure 5.9. As expected, the estimate of v_x can be considered to be perfect. Even though $\hat{v}_y$ suffers some degradation during the slalom maneuver, it has been corrected for the RBA disturbance, which is the main purpose of the augmented observer. v_y^{GPS} can be seen to contain a good deal of noise, but very little of this passes through to $\hat{v}_y$, implying observer robustness with regards to high frequency noise.

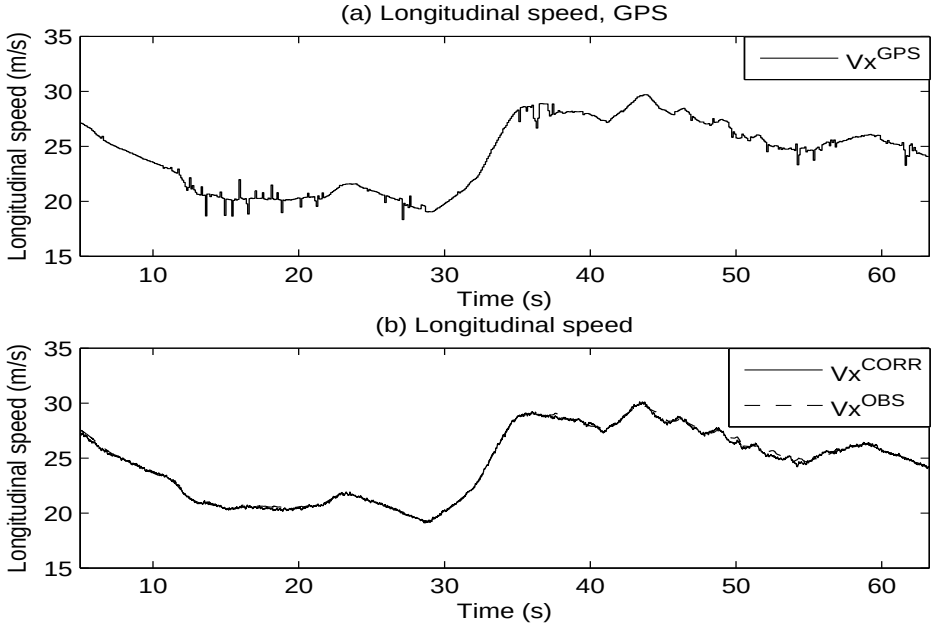

Figure 5.9: (a) v_x^{GPS} (b) Actual v_x and $\hat{v}_x$, augmented observer

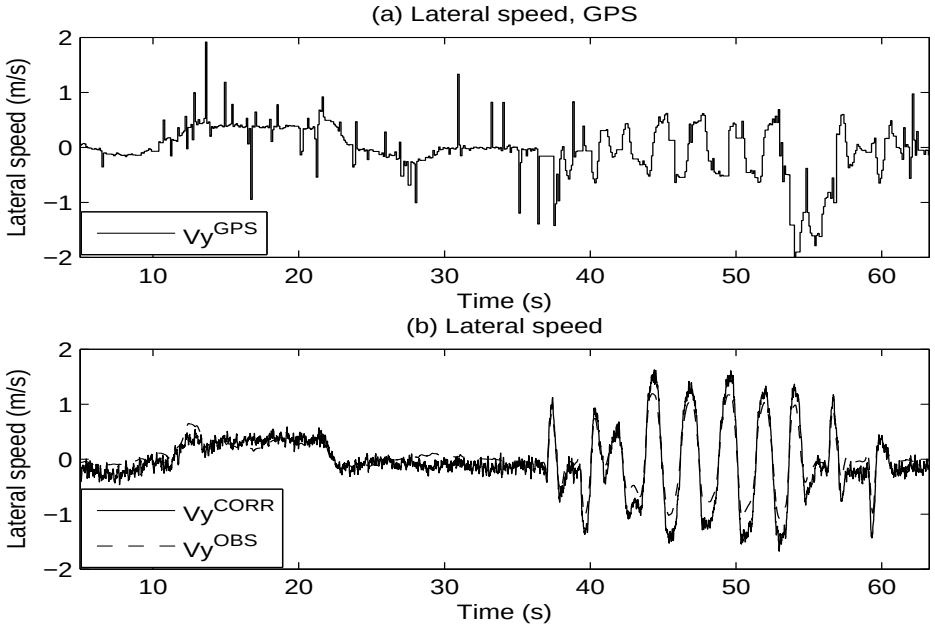

Figure 5.10: (a) v_y^{GPS} (b) Actual v_y and $\hat{v}_y$, augmented observer

It has been mentioned several times that the v_y^{GPS} can get extremely noisy. Because of this, it is necessary to see how the augmented observer behaves when this happens. The test from Figure 5.5 and Figure 5.6 is evaluated again, this time using the augmented observer with feedback from a noise-ridden v_y^{GPS}. See Figure 5.11 and Figure 5.12. Once again it can be seen that the high-frequency components of v_y^{GPS} have very little effect on $\hat{v}_y$. If a larger value of K_{w_ϕ} was chosen, a larger degradation of $\hat{v}_y$ would be seen.

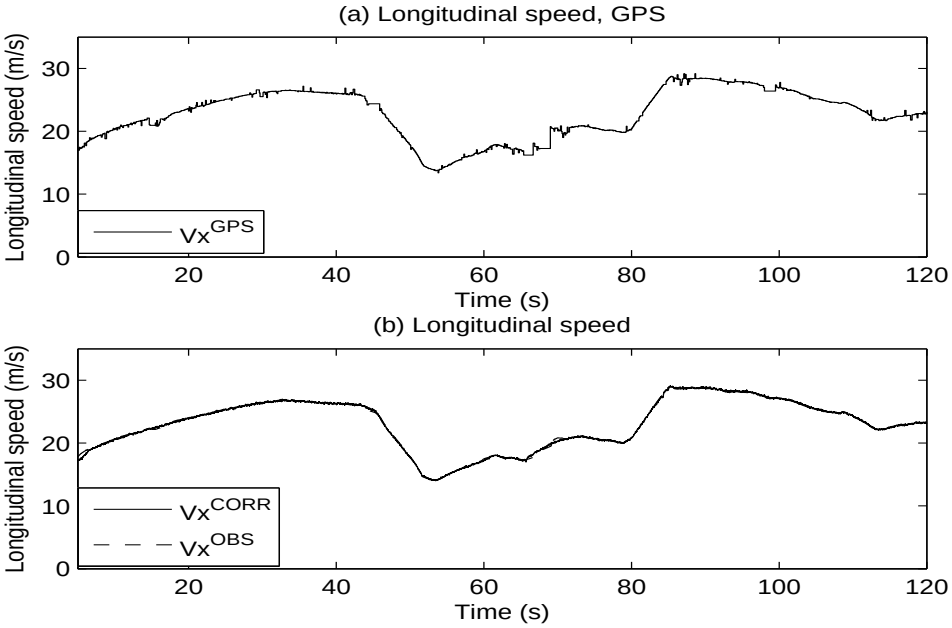

Figure 5.11: (a) v_x^{GPS} (b) Actual v_x and $\hat{v}_x$, augmented observer

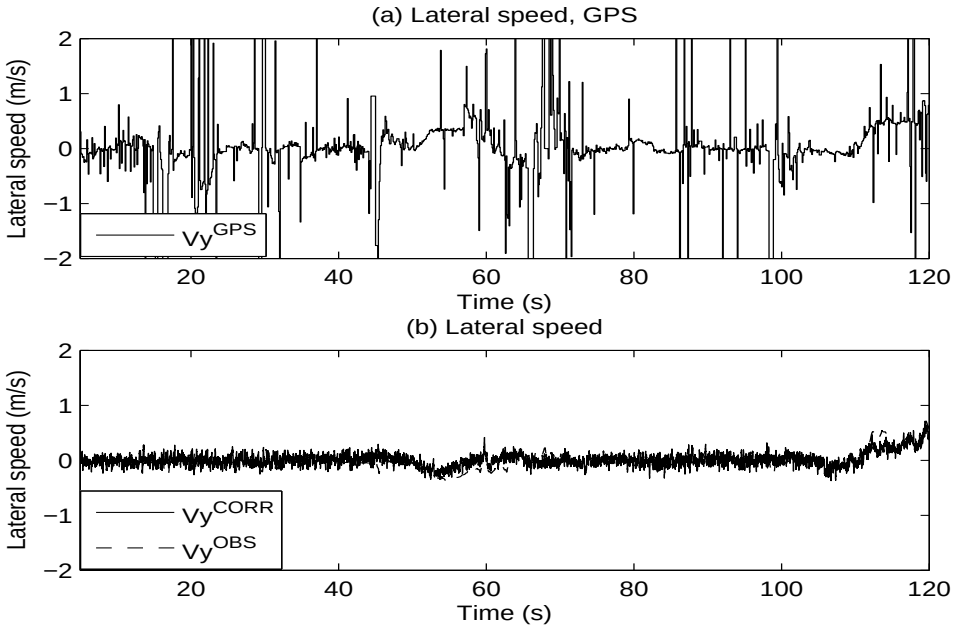

Figure 5.12: (a) v_y^{GPS} (b) Actual v_y and $\hat{v}_y$, augmented observer

To see exactly how accurate the RG and RBA compensation is, it is constructive to evaluate performance when both a_x and a_y are biased by simulated gravity components, much like in Figure 5.8. To minimize disturbances caused by driving pattern, a data set for a stand-still test will be considered. Adding a sinusoidal bias to the acceleration measurements, corresponds to placing the vehicle on a tiltable platform. Since velocity and slip are both zero, the results will not be affected by errors in the friction model. Figure 5.13 shows what happens to the non-adaptive observer when a_x and a_y are affected by the same bias; in this case a sinus with amplitude corresponding to RG and RBA of 10 degrees. Even when the vehicle isn't moving, the acceleration bias causes a relatively large error in the velocity estimates. Figure 5.14 demonstrates how the augmented observer deals with the problem.

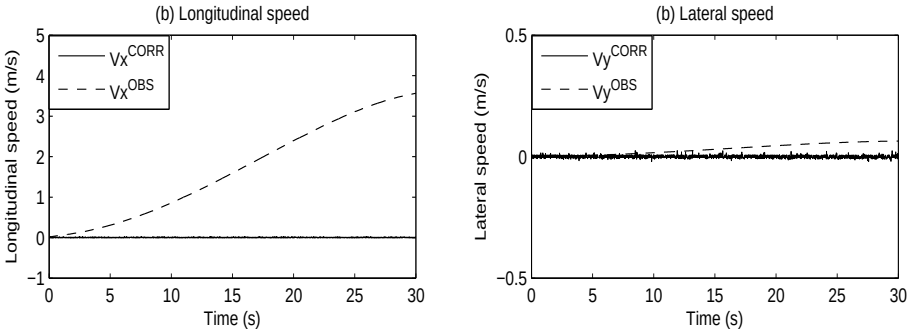

Figure 5.13: (a) Actual v_x and $\hat{v}_x$, non-adaptive (b) Actual v_y and $\hat{v}_y$, non-adaptive

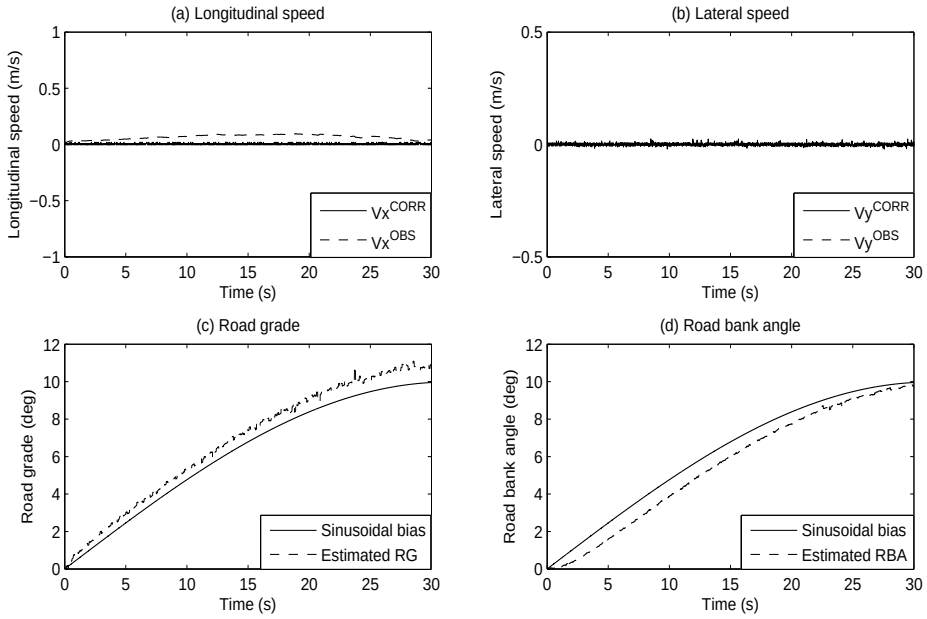

Figure 5.14: (a) Actual v_x and $\hat{v}_x$, augmented (b) Actual v_y and $\hat{v}_y$, augmented (c) Acceleration bias and estimated RG (d) Acceleration bias and estimated RBA

Clearly, the augmented observer has better performance when the assumption of flat surface driving no longer holds. While the estimates of RG and RBA are slightly skewed, they account for velocity errors quite nicely. The error observed in $\hat{v}_x$ is less than 0.1 m/s, and in effect negligible.

The test results presented in this section show that **Criterion 3** holds, even though many more tests should be performed for a definite conclusion to be made. Ideally, all the data sets should contain information about road structure, making verification of observer correctness (or failure) easier.

5.4 Criterion 4

Criterion 4 is tested using the physically accurate CASCaDE simulator, in which all relevant parameters can be adjusted manually. Roll and bank angle compensation is tested for basic maneuvers on varying surface conditions. There is one large disadvantage with these tests - a simulator can't fully represent real life physics or sensor configurations. It does, however, help in determining feasibility of suggested solutions.

The roll rate measurement is simulated by the Euler rate $\dot{\phi}$ which is available in CASCaDE. This will be a good approximation as long as Euler angle $\theta = 0$. When the vehicle experiences sideslip on a banked road, this won't be the case, meaning that certain results need a more thorough examination than others.

5.4.1 Roll compensation

In this section, performance of the roll compensated observer from section 4.4 is tested for steady turn and slalom maneuvers. The goal is to determine if roll compensation can lead to improvements in $\hat{v}_y$. All tests are performed without friction adaptation, using longitudinal speed $v_x = 80$ km/h and feedback gains set to 1. Variables used:

ϕ – Actual Euler angle, as given by CASCaDE

ϕ^{OBS} – Estimated roll angle without roll compensation

$\phi^{OBS\phi}$ – Estimated roll angle with roll compensation

v_y – Actual lateral speed, as given by CASCaDE

$v_y{}^{OBS}$ – Estimated lateral speed without roll compensation

$v_y{}^{OBS\phi}$ – Estimated lateral speed with roll compensation

Figures 5.15, 5.16, 5.17 indicate that roll compensation probably isn't necessary when there is no bank angle. $\hat{v}_y$ is degraded for high friction conditions, and slightly improved for low friction conditions, which means that the essence lies in how K_{v_y} is tuned, not how a_y is modified. This is an expected result, as dynamic roll is proportional to lateral acceleration, and can be corrected for by simply scaling the acceleration measurement.

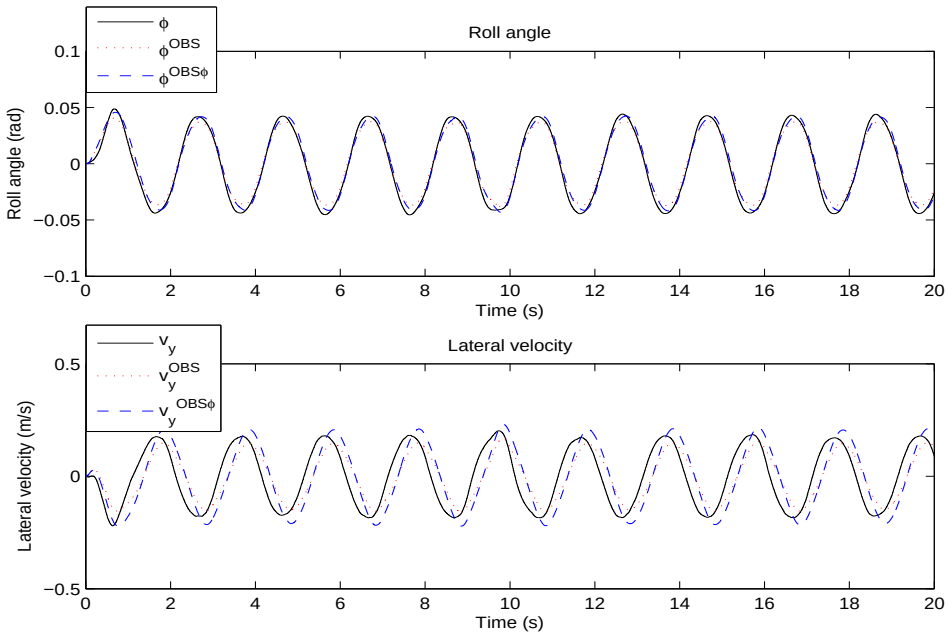

Figure 5.15: Slalom maneuver, $\mu_H = 1$

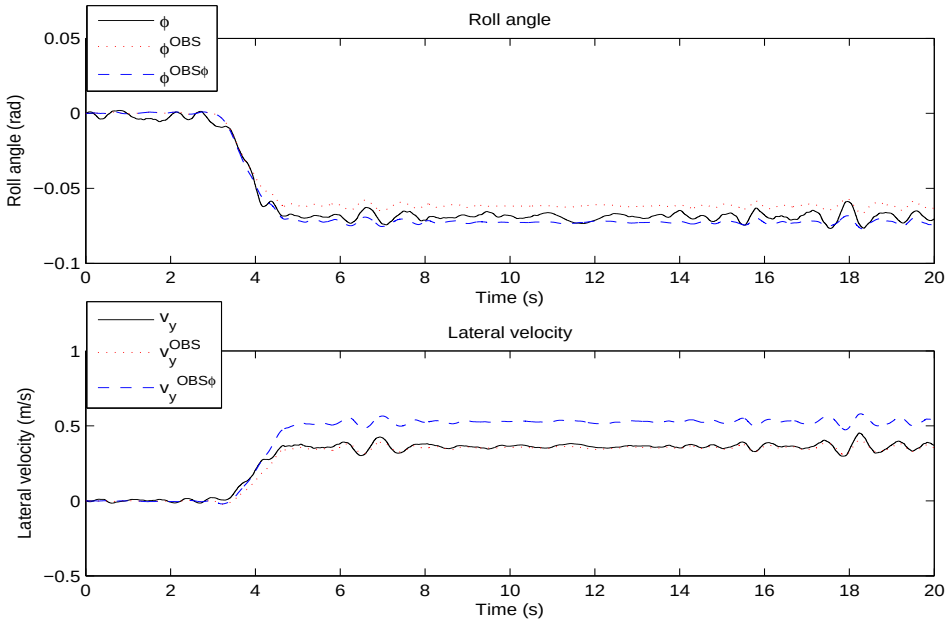

Figure 5.16: Steady turn, $\mu_H = 1$

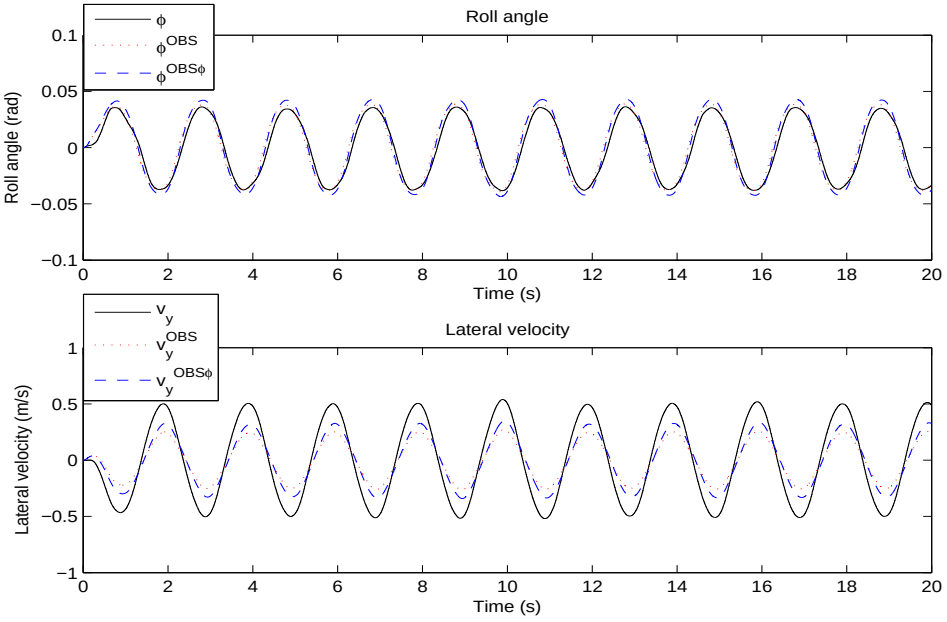

Figure 5.17: Slalom maneuver, $\mu_H = 0.5$

5.4.2 Road bank angle compensation

As bank angle compensation is the main focus of this report, performance of the observer in section 4.4.1 is of great interest. If an arbitrary percentage of the accelerometer bias due to RBA can be removed, a corresponding improvement in $\hat{v}_y$ can be expected. Because stability of the RBA observer hasn't been determined mathematically, these results should only be viewed as indicators of practical usefulness, not validations of presented theory. The RBA estimate itself is just the integral of the difference between measured and estimated roll rate, and will likely diverge over time if used directly. This problem is left untreated for the time being.

Figures 5.18 and 5.19 demonstrate how the RBA estimate can be used to correct large gravitational biases in the accelerometer. Of course an RBA value of 0.12 rad, which is about 7 degrees, represents a completely unrealistic driving condition, but it shows that the observer is able to handle regular roads.

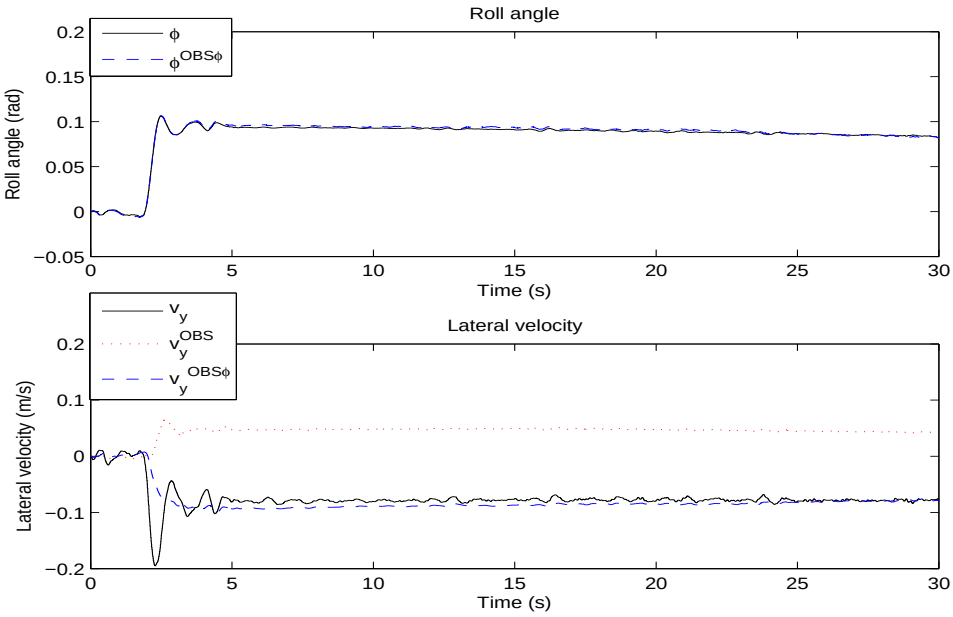

Figure 5.18: Straight drive with change in RBA after two seconds, RBA = 0.12 rad, $\mu_H = 1$

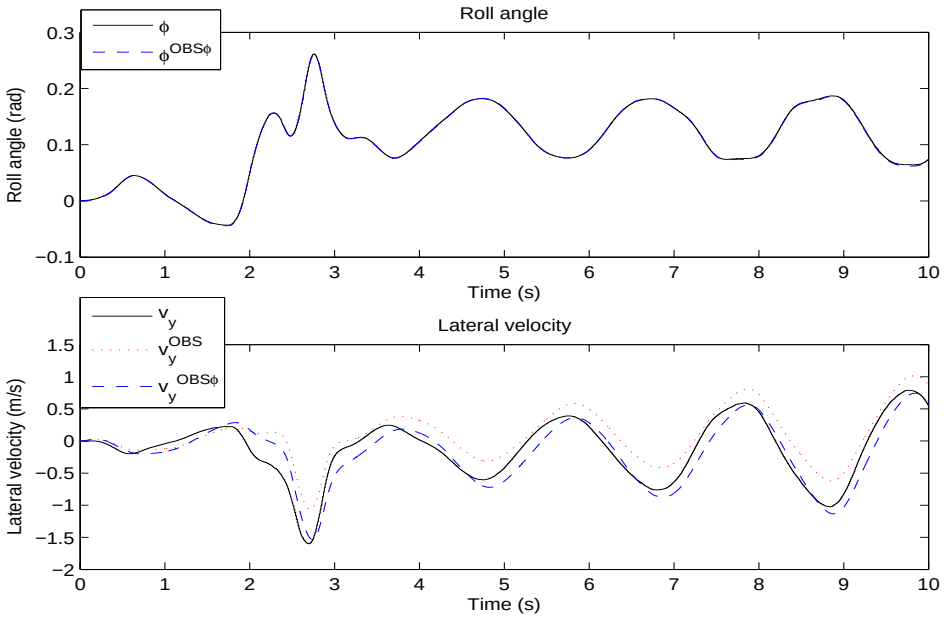

Figure 5.19: Slalom maneuver with change in RBA after two seconds, RBA = 0.12 rad, $\mu_H = 1$

In Figure 5.20 it can be seen that $\phi^{OBS\phi}$ deviates from ϕ. The exact reasons for this can't be identified, but a contributing factor is vehicle sideslip. Recalling that ϕ is the Euler angle, one can deduce that it will be smaller than the bank angle when the vehicle experiences sideslip. The observer, however, has no mechanism for sideslip compensation, an improvement that will be necessary in a practical implementation. Either way, estimated lateral velocity is better than without RBA compensation.

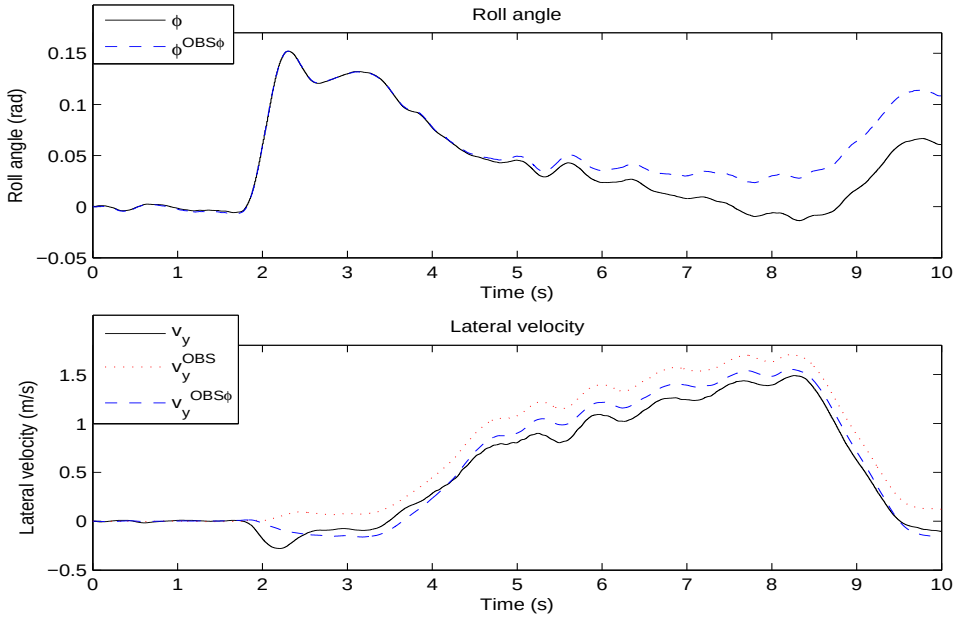

Figure 5.20: Right-left turning maneuver with change in RBA after two seconds, RBA = 0.12 rad, $\mu_H = 1$

Figures 5.21 and 5.22 demonstrate what happens when the friction parameter μ_H is set to 0.5 instead of 1. For the slalom maneuver, estimated RBA is correct and $\hat{v}_y$ improved, although $\hat{v}_y$ is too conservative for the slippery surface conditions. (Observer tuning is not considered an important aspect of this report - the main focus lies in getting estimates that mimimc reality in terms of shape.) For the slower right-left maneuver, a deviation affects the RBA estimate. Like before, it is hard to determine exactly what happens, but it most likely has to do with sideslip and vehicle orientation on the surface. These conditions break Assumption 4.8 and will have to be considered in future observer improvements. By letting the vehicle perform a longer left turn, the result is as shown in Figure 5.23.

It is clear that the RBA observer has merit. A simulator can't recreate reality, so there's obviously need for testing and tuning on a vehicle, but as an initial indicator, the presented results are positive.

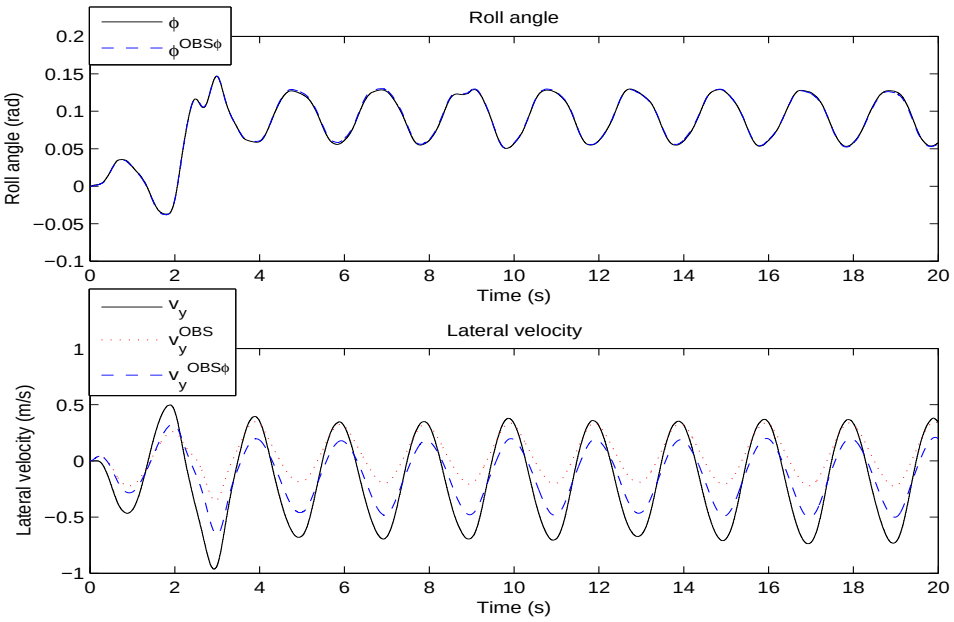

Figure 5.21: Slalom maneuver with change in RBA after two seconds, RBA = 0.087 rad, $\mu_H = 0.5$

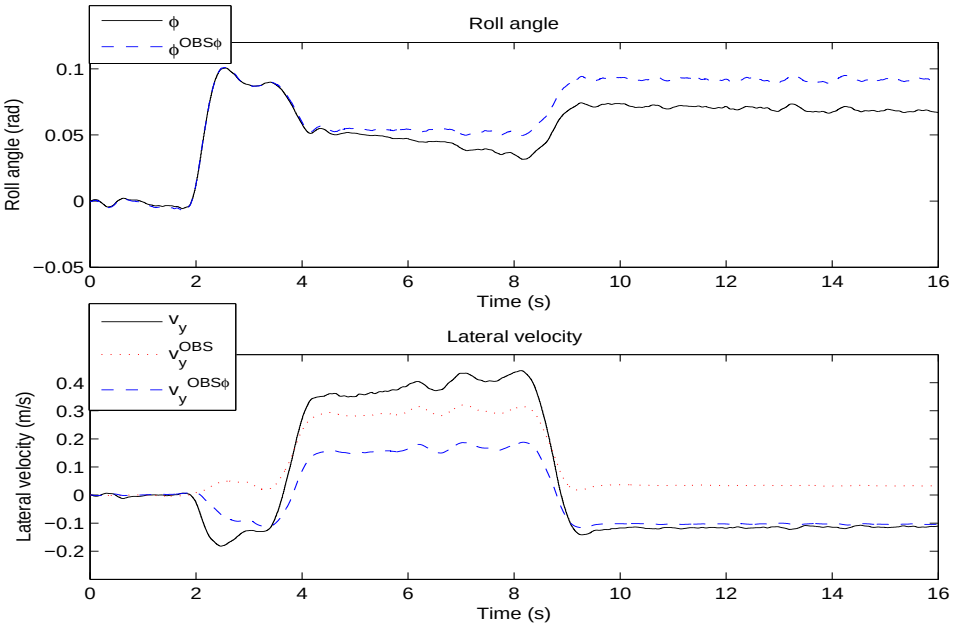

Figure 5.22: Left-right turning maneuver with change in RBA after two seconds, RBA = 0.087 rad, $\mu_H = 0.5$

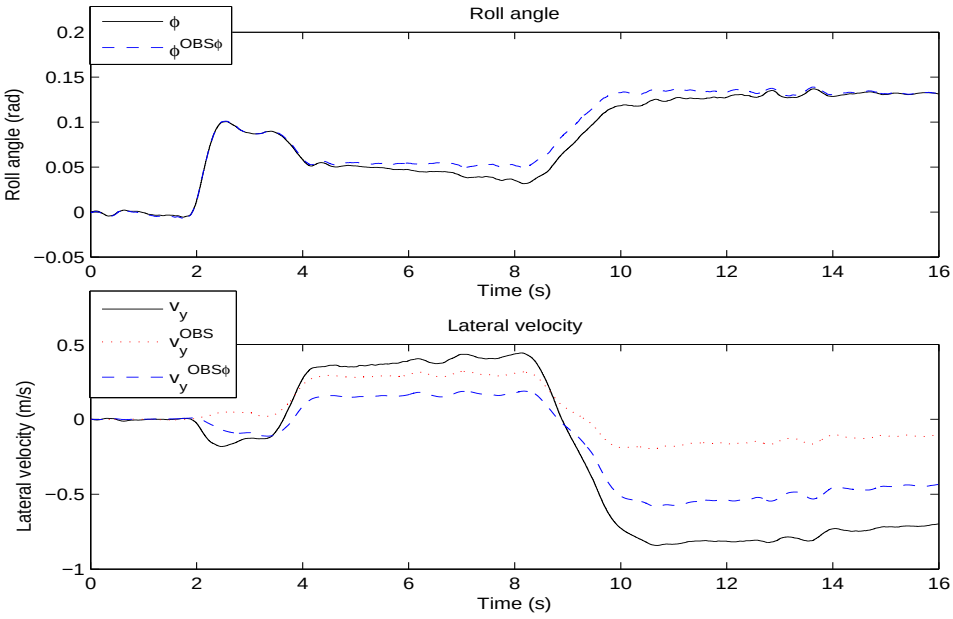

Figure 5.23: Left-right turning maneuver with change in RBA after two seconds, RBA = 0.087 rad, $\mu_H = 0.5$

Chapter 6

Conclusion

In this report, an approach to estimating road grade and road bank angle, using GPS as an aiding system, has been presented, together with an approach to bank angle estimation using a roll rate gyro as measurement. The interest in this stems from the knowledge that existing nonlinear observers for vehicle state estimation have weaknesses with regards to these disturbances. Firstly, it has been shown that calculating vehicle velocity from GPS position measurements is a straightforward procedure, although far from ideal with regards to noise and accuracy. Furthermore, the GPS measurements suffer from a time delay which is too large for them to be used in a stand-alone implementation. However, simple filtering techniques have been demonstrated to give good enough signals for integration with a nonlinear observer. Secondly, augmentations to a previously developed nonlinear observer has been made, so that it is able to make use of the new information that GPS provides. Also, the development of a mathematical model for vehicle roll has made bank angle detection possible through the aid of a gyro measurement. Stability of the augmented observer has not been proven for a general set of constrained feedback-gains, but it has been shown that stability is ensured when certain assumptions about the physical system holds. The same is true for the roll observer without bank angle compensation. However, no stability proof is presented for the bank angle parameter estimate. Finally, it has been demonstrated that the augmented observer gives good estimates of road grade and road bank angle, and accounts for the errors they cause when not compensated for, through evaluation of data from actual vehicle tests. While the augmented observer suffers some degradation of performance when no disturbances are present, the overall increase in robustness is good enough to consider it an improvement over existing solutions. The gyro based bank angle observer shows potential, and should be considered for implementation on a test vehicle.

The main focus of this report has been to determine if it is feasible to use GPS as an aiding system for vehicle state estimation with nonlinear observers, and if the problems related to bank angle can be partially removed using a simpler measurement unit, such as a roll rate gyro. For the GPS problem, the conclusion is obvious: By in-

corporating relatively poor GPS velocity measurements in the feedback loop, a notable increase in estimation performance during periods of road disturbance is gained. This clearly demonstrates feasibility of the proposed solution. Bank angle estimation by aid of a roll gyro also looks promising, but because stability proofs and actual vehicle tests are lacking, no final conclusions can be made at this point. Note that although the presented results are positive, they should not be regarded as optimal. For the augmented observer to be implemented in an actual vehicle, it would need modifications and improvements which haven't been considered in this report. Notwithstanding, the ability to account for disturbances such as road grade and road bank angle, makes it successful in laying a foundation for future solutions. The same can be said for the less rigorously tested bank angle observer.

Appendix A

Kinematics

A.1 Rotation matrix

The rotation matrix **R** between two frames a and b is denoted as $\mathbf{R}_b^a$, and it is an element in $SO(3)$, which is the special orthogonal group of order 3:

$$SO(3) = \{\mathbf{R} | \mathbf{R} \in \mathbb{R}^{3\times 3}, \mathbf{R} \text{ is orthogonal and det}\mathbf{R} = 1\} \tag{A.1}$$

The group $SO(3)$ is a subset of all orthogonal matrices of order 3, $SO(3) \subset O(3)$, where $O(3)$ is defined as:

$$O(3) = \{\mathbf{R} | \mathbf{R} \in \mathbb{R}^{3\times 3}, \mathbf{R}\mathbf{R}^T = \mathbf{R}^T\mathbf{R} = \mathbf{I}\} \tag{A.2}$$

Appendix B

MATLAB functions

B.1 Butter

BUTTER - Butterworth digital and analog filter design. [B,A] = BUTTER(N,Wn) designs an Nth order lowpass digital Butterworth filter and returns the filter coefficients in length N+1 vectors B (numerator) and A (denominator). The coefficients are listed in descending powers of z. The cutoff frequency Wn must be 0.0 < Wn < 1.0, with 1.0 corresponding to half the sample rate.

B.2 Pwelch

PWELCH - Power Spectral Density estimate via Welch's method. Pxx = PWELCH(X) returns the Power Spectral Density (PSD) estimate, Pxx, of a discrete-time signal vector X using Welch's averaged, modified periodogram method. By default, X is divided into eight sections with 50window and eight modified periodograms are computed and averaged.

Bibliography

[1] A.T. van Zanten. Bosch esp system: 5 years of experience. *Proceedings of the Automotive Dynamics & Stability Conference*, Paper no. 2000-01-1633, 2000.

[2] Jim Farrelly and Peter Wellstead. Estimation of vehicle lateral velocity. *Proceedings of the 1996 IEEE International Conference on Control Applications*, pages 552–557, 1996.

[3] Lars Imsland, Tor A. Johansen, Thor I. Fossen, Håvard Fjær Grip, Jens C. Kalkkuhl, and Avshalom Suissa. Vehicle velocity estimation using nonlinear observers. *Automatica*, 2006.

[4] Håvard Fjær Grip, Lars Imsland, Tor A. Johansen, Thor I. Fossen, Jens C. Kalkkuhl, and Avshalom Suissa. Nonlinear vehicle velocity observer with road-tire friction adaptation. *Automatica*, 2006.

[5] David M. Bevly, J. Christian Gerdes, Christopher Wilson, and Gengsheng Zhang. The use of gps based velocity measurments for improved vehicle state estimation. *Proceedings of the American Control Conference, Chicago, Illinois*, June:2538–2542, 2000.

[6] David M. Bevly, Robert Sheridan, and J. Christian Gerdes. Integrating ins sensors with gps velocity measurments for continuous estimation of vehicle sideslip and tire cornering stiffness. *Proceedings of the American Control Conference, Arlington, VA*, June 25-27:25–30, 2001.

[7] David M. Bevly, J. Christian Gerdes, and Christopher Wilson. The use of gps based velocity measurments for measurment of sideslip and wheel slip. *Vehicle System Dynamics*, 38:127–147, 2002.

[8] Robert Daily and David M. Bevly. The use of gps for vehicle stability control systems. *IEEE Transactions on industrial electronics*, 51, N0. 2, April:270–277, 2004.

[9] David M. Bevly. Global positioning system (gps): A low-cost velocity sensor for correcting intertial sensor errors on ground vehicles. *Journal of Dynamic Systems, Measurment, and Control*, June 2004:255–264, 2004.

[10] Jihan Ryu and J. Christian Gerdes. Integrating inertial sensors with gps for vehicle dynamics control. *Journal of Dynamic Systems, Measurment, and Control*, June:1–26, 2004.

[11] H.E. Tseng. Dynamic estimation of road bank angle. *Vehicle System Dynamics*, 36, No. 4-5:307–328, 2001.

[12] Hong S. Bae, Jihan Ryu, and J. Christian Gerdes. Road grade and vehicle parameter estimation for longitudinal control using gps. *IEEE Conference on Intelligent Transportation Systems*, 2001.

[13] Jihan Ryu and J. Christian Gerdes. Estimation of vehicle roll and road bank angle. *Proceeding of the 2004 American Control Conference*, June:2110–2115, 2004.

[14] Thor I. Fossen. *Marine Control Systems*. Marine Cybernetics, 2002.

[15] Olav Egeland and Jan Tommy Gravdahl. *Modeling and Simulation for Automatic Control*. Marine Cybernetics, 2000.

[16] Brad Schofield. Vehicle dynamics control for rollover prevention. Licentiate Thesis ISRN LUTFD2/TFRT--3241--SE, Department of Automatic Control, Lund University, Sweden, December 2006.

[17] Jay A. Farrell and Matthew Barth. *The Global Positioning System & Inertial Navigation*. McGraw-Hill, 1998.

[18] Chris Rizos. Notes on basic gps positioning and geodetic concepts. http://www.gmat.unsw.edu.au, 1999.

[19] United States Government. Current gps constellation. http://tycho.usno.navy.mil, 2006.

[20] Bradford W. Parkinson and James J. Spilker Jr. *Global Positioning System: Theory and Applications Volume II*. American Institute of Aeronautics and Astronautics, INC, 1996.

[21] Donghyun Kim and Richard B. Langley. Gps ambiguity resolution and validation: Methodologies, trends and issues. GPS Research Group Geodetic Research Laboratory, Department of Geodesy and Geomatics Engineering University of New Brunswick, Fredericton, N.B. E3B 5A3, Canada, 2000.

[22] Yang Yunchun, Hatch R. R., and Sharpe R. T. Minimizing the integer ambiguity search space for rtk. NavCom Technology, Inc., 2003.

[23] Sebum Chun, Chulbum Kwon, Eunsung Lee, Young-Jae Lee, and Taesam Kang. Performance analysis of gps integer ambiguity resolution using external aiding information. In *The 2004 International Symposium on GNSS/GPS*, 2004.

[24] John G. Proakis and Dimitris G. Manolakis. *Digital Signal Processing*. Prentice Hall International, Inc., 1996.

[25] Lars Imsland, Tor A. Johansen, Håvard Fjær Grip, and Thor I. Fossen. On non-linear unknown input observers - applied to lateral vehicle velocity estimation on banked roads. *International Journal of Control*, 2006.

[26] Håvard Fjær Grip. Nonlinear vehicle velocity observer with road-tire friction adaptation. NTNU, 2006.

[27] Hassan K. Khalil. *Nonlinear Systems*. Prentice-Hall, 2000.

[28] Chi-Tsong Chen. *Linear System Theory and Design*. Oxford University Press, 1999.